From Spheroids to Bioprinting: A Literature Review on Biomanufacturing strategies of 3D In vitro Osteosarcoma Models

Margarida Domingues[1,2], João C. Silva[1,2], and Paola Sanjuan-Alberte[1,2]

[1]Department of Bioengineering and Institute for Bioengineering and Biosciences, Instituto Superior Técnico, Universidade de Lisboa, Av. Rovisco Pais, 1049-001 Lisbon, Portugal
[2]Associate Laboratory i4HB—Institute for Health and Bioeconomy, Instituto Superior Técnico, Universidade de Lisboa, Av. Rovisco Pais, 1049-001 Lisbon, Portugal

April 23, 2024

Abstract

Osteosarcoma (OS) is a rare primary malignant bone cancer affecting mainly young individuals. Treatment typically consists of chemotherapy and surgical tumor resection, which has undergone few improvements since the 1970s. This therapeutic approach encounters several limitations attributed to the tumor's inherent chemoresistance, marked heterogeneity and metastatic potential. Therefore, the development of *in vitro*platforms that closely mimic the OS pathophysiology is crucial to understand tumor progression and discover effective anticancer therapeutics. Contrary to 2D monolayer cultures and animal models, 3D*in vitro* platforms show promise in replicating the 3D tumor macrostructure, cell-cell and cell-extracellular matrix interactions. This review provides an overview of the biomanufacturing strategies employed in developing 3D *in vitro* OS models, highlighting their role in replicating different aspects of OS and improving OS anticancer research and drug screening. A variety of 3D *in vitro* models are explored, including both scaffold-free and scaffold-based models, encompassing cell spheroids, hydrogels, and innovative approaches like electrospun nanofibers, microfluidic devices and bioprinted constructs. By examining the distinctive features of each model type, this review offers insights into their potential transformative impact on the landscape of OS research and therapeutic innovation, addressing the challenges and future directions of 3D *in vitro* OS modeling.

1. Introduction

Osteosarcoma (OS) is the most common type of primary bone sarcoma, characterized by an abnormal production of osteoid matrix by tumor cells. [1] Unlike carcinomas, which are the most common malignant tumors and develop in epithelial tissues, sarcomas are rare and develop in connective tissues, namely bone and soft tissues, such as muscle, cartilage, fat and blood vessels.[2] About 3.4 cases per million people are diagnosed with OS each year, which accounts for 1% and 3-5% of all new cancer diagnoses in adults and children, respectively.[2,3,4] OS presents a bimodal age distribution, having a significant peak incidence in children and adolescents with ten to fourteen years of age, and a second less pronounced peak in adults over the age of sixty. [1]

While OS may occur in any bone, it is more frequently found in the metaphysis of long bones, such as the femur (30%), tibia (15%) and humerus (15%). [5] The metaphysis contains the growth plate, which is the region where the longitudinal growth of the bone occurs, and, therefore, holds the highest percentage of proliferative cells in the entire bone. [6]Besides the primary bone tumor, OS commonly presents with metastases, especially in the lungs (80-90%). [7]

Common symptoms of OS include discomfort or pain in the affected area, limited joint mobility and a palpable growing mass.[4] Imaging techniques, such as X-Ray and magnetic resonance imaging (MRI), typically show the presence of a poorly marginated bone with deposition of mineralized matrix and zones of resorption. Ultimately, the diagnosis is made with a biopsy, which must reveal a large mass of malignant spindle-like cells with pleomorphic nuclei, and disorganized osteoid production. [8]Based on the predominant type of matrix-producing cells, OS can be subclassified as osteoblastic, fibroblastic or chondroblastic, although the prognosis is virtually the same. [4,5]

Even though around 95% of cases appear spontaneously, a few risk factors for OS have been identified. These include rapid bone growth during puberty, bone exposure to radiation, pre-existing bone diseases and other heritable genetic syndromes, such as Li-Fraumeni syndrome (LFS). [9] In fact, 12% of people diagnosed with LFS, which occurs due to a germline mutation of the TP53 gene, will develop OS in their lifetime. [10]

The treatment plan for OS has not changed significantly in the last four decades, consisting of surgical tumor resection combined with adjuvant and neoadjuvant chemotherapy. [1,5] Currently, about 85 to 90% of tumor resections can be made through limb-salvaging surgeries, with amputation being reserved for non-resectable tumors.[3] The chemotherapy used is referred to as MAP-therapy, as it involves the use of the cytotoxic drugs methotrexate, adriamycin (doxorubicin) and platinol (cisplatin).[5] Recently, ifosfamide has also been combined with these cytotoxic agents. [3] When it was first introduced in the 1970s, the combination of chemotherapy with conservative surgery to treat OS initially increased its survival rate. However, this course of treatment is currently not effective, mainly due to chemoresistance and the metastatic spread of the tumor, leading to a stagnant survival rate over the years: [1]according to the American Cancer Society, [11] as of 2023, the 5-year survival rate in the United States for localized OS is 76%, which decreases to 24% for metastatic OS. Moreover, it is estimated that 20% and 80% of patients with localized and metastatic disease, respectively, will experience cancer recurrence within the first three years after treatment. [4]

The development of OS cannot be explained by a single genetic event. Instead, it is typically associated with several genetic and epigenetic changes, being influenced by bone microenvironmental signals as well.[5] The most common mutations in OS are found in the TP53 and retinoblastoma (RB) tumor suppressor genes, which encode for the p53 and RB proteins, respectively. The p53 protein is a nuclear transcription factor that prevents the propagation of cells with serious DNA damage. This is achieved by either arresting the cell cycle, allowing cells to repair their DNA damage, or by initiating apoptosis if the damage is irreparable. [12] Similarly, activation of the RB protein, in response to environmental changes, including DNA damage, also results in cell cycle arrest, as this protein inhibits gene transcription, which is required for the cell to enter the S-phase of the cell cycle. [13]

Several cell types along the mesenchymal-osteogenic lineage have been proposed as the OS cell-of-origin, i.e., the normal cells that initially acquire the mutations that promote tumor development.[5] These include the mesenchymal stem/stromal cells (MSCs), which are primarily found in the bone marrow and can differentiate into multiple lineages, including the osteogenic, chondrogenic, myogenic and adipogenic lineages. [14] While *in vitro* studies showed that inactivation of the TP53 gene in non-osteogenic committed MSCs was able to generate OS, the highest incidence was found when such mutations were induced in osteoblastic MSC precursors and mature osteoblasts. This shows that MSCs that undergo osteoblastic differentiation are more likely to be involved in the initial development of OS. [5]

The accumulation of such mutations in MSCs and their progenitors has been linked to the formation of OS cancer stem cells (CSCs), also referred to as tumor-initiating cells, which are able to self-renew, differentiate and support tumor growth, by interacting with the extracellular matrix (ECM). [5,15,16]Additionally, they are highly resistant to chemotherapy due to their enhanced ability to repair DNA damages and remove drugs from their cytoplasm, being responsible for tumor relapses and metastasis.[17,18] As such, recent strategies have been focused on targeting OS-CSCs and their microenvironment.

To understand the pathophysiology of OS and discover more effective therapeutic strategies, it is imperative to establish robust preclinical models capable of evaluating their efficacy prior to clinical trials. Traditional

approaches include 2D *in vitro* models and *in vivo* animal models, yet they present major limitations. Notably, 2D cultures lack relevant interactions between tumor cells and the 3D macrostructure of the tumor, while animal models typically raise ethical concerns. [19, 20] Addressing these challenges, 3D*in vitro* models have emerged as promising preclinical alternatives. In this review, we provide a comprehensive overview of the strategies that have been employed to develop 3D *in vitro* models of OS. Specifically, we focus on bioengineering approaches that contribute towards the biomimicry of the OS tumor microenvironment, through the use of scaffolds, and how innovative manufacturing techniques, such as electrospinning, microfluidics and 3D bioprinting, can be valuable resources for researchers in the field of OS modeling.

2. Modeling the complexity of OS

2.1. Bone tissue and homeostasis

The bone tissue contains a variety of cell types and a mineralized ECM, composed of organic (40%) and inorganic (60%) phases.[21] The organic phase is mainly composed of collagen type I (90%), which is organized in fibrils and provides mechanical support. The remaining non-collagenous proteins include proteoglycans (e.g., aggrecan, versican and decorin), glycoproteins (e.g., fibronectin, laminin and osteopontin), Gla-containing proteins (e.g., osteocalcin and Matrix Gla protein), cytokines (e.g., interleukin (IL)-6 and tumor necrosis factor (TNF)-α) and growth factors (e.g., transforming growth factor (TGF)-β and insulin-like growth factor (IGF)-1). [22,23] The inorganic phase, which is deposited within the collagen fibrils, mostly consists of calcium phosphate in the form of hydroxyapatite [$\mathbf{Ca_{10}(PO_4)_6(OH)_2}$], being responsible for mineral exchange.[21,22,24].

The bone resident cells refer to osteoblasts, osteocytes and osteoclasts, which interact with each other and the surrounding matrix. This crosstalk is important for the bone remodeling process, in which the bone tissue is renewed. [14] Bone production is performed by osteoblasts, which arise from mesenchymal stem/stromal cells differentiation, and includes the release of ECM components, namely collagen and proteoglycans, and extracellular vesicles (EVs) that contain alkaline phosphatase, important in the mineralization of the newly synthesized matrix. [22] The term "osteocyte" refers to osteoblasts that become entrapped within the bone matrix during this process. These cells are the main mechanoreceptors of bone, secreting paracrine factors in response to mechanical stresses. [25] Bone resorption is carried out by osteoclasts, which are multinucleated cells, differentiated from monocytes and macrophages, that dissolve the bone minerals and digest the ECM components, mainly by releasing matrix metalloproteinases (MMPs). [26]

Under normal conditions, there is a balance between the osteoblastic and osteoclastic activity of bone cells to ensure homeostasis, which is primarily regulated by the RANKL/RANK/OPG pathway.[27] The receptor activator of nuclear factor k-B ligand (RANKL), which is secreted by osteoblasts, binds to its receptor RANK, found in osteoclast progenitors, and promotes the differentiation of preosteoclasts into osteoclasts, which leads to bone resorption. As a result, TGF-β is released, which stimulates the migration of MSCs to the bone environment and their differentiation into osteoblasts. By releasing osteoprotegerin (OPG), which binds to RANLK, osteoblasts inhibit RANK signaling and bone resorption. [28]

2.2 Bone Tumor Microenvironment

Tumor cells proliferate, migrate and resist apoptosis in a complex and dynamic environment, known as the tumor microenvironment (TME).[24] As OS develops within the bone tissue, its TME is naturally composed of a densely mineralized ECM surrounding the cellular milieu, which includes tumor and bone cells.

OS cells secrete pro-osteoclastic factors, such as RANKL, that promote osteoclastogenesis. The resulting excessive bone resorption leads to the release of factors previously entrapped in the bone matrix, such as IGF-1 and TGF-β, which will, in turn, promote tumor proliferation.[29] Additionally, OS cells secrete

pro-osteoblastic factors, including parathyroid hormone-related protein (PTHrP), that contribute to an increased expression of RANKL as well as the secretion of pro-tumor growth factors, such as IL-6 and vascular endothelial growth factor (VEGF). [9] Altogether, the normal bone remodeling process is disrupted, allowing the creation of a microenvironment that supports the development of the tumor.[29,30] Besides OS and bone resident cells, other cell types are present within the OS-TME, including vascular cells (endothelial and perivascular cells), stromal cells (MSCs and fibroblasts) and immune cells (macrophages and lymphocytes), which also have important roles in key events of tumor growth, including ECM remodeling, neovascularization and migration,[21,31] as illustrated in Figure 1.

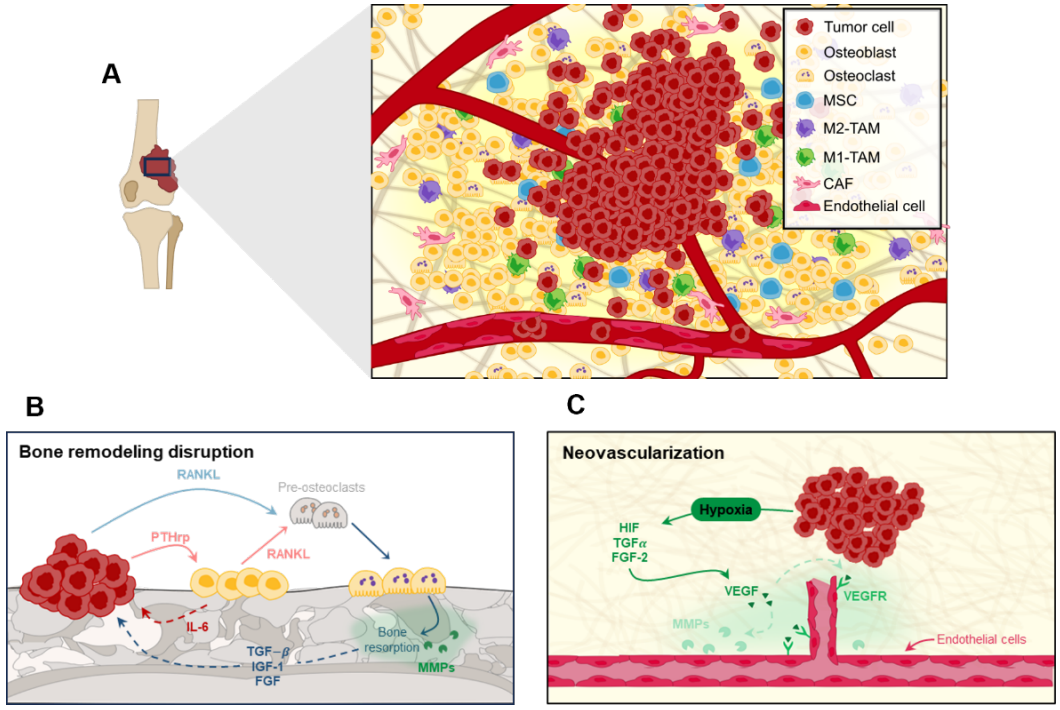

Figure 1. Graphical representation of the OS-TME and relevant processes for tumor progression. (A) Bone TME, including the cellular niche, the surrounding ECM and the vasculature that supports the tumor; (B) Bone remodeling disruption by tumor cells and the consequent ECM remodeling by osteoclasts which favors tumor proliferation; (C) Characteristic neovascularization of bone tumors, which includes the sprouting of endothelial cells, promoted by VEGF, whose expression is increased in a hypoxic environment. MSC: mesenchymal stromal/stem cell; M1-TAM: M1-polarized tumor-associated macrophage; M2-TAM: M2-polarized tumor-associated macrophage; CAF: cancer-associated fibroblast; RANKL: receptor activator of nuclear factor k-β ligand; PTHrP: parathyroid hormone-related protein; IL-6: Interleukin-6; TGF: Transforming growth factor; IGF: Insulin-like Growth Factor; FGF: Fibroblast Growth Factor; MMPs: Matrix Metalloproteinases; HIF: Hypoxia-inducible Factor; VEGF: Vascular Endothelial Growth Factor; VEGFR: Vascular Endothelial Growth Factor Receptor.

As with any type of tumor, the rapid and unrestricted growth of OS cells leads to a depletion of oxygen and the resulting hypoxic microenvironment promotes the overexpression of hypoxia-inducible factor (HIF), which increases the expression of glycolysis-related molecules. OS cells are thus forced to change their metabolism from oxidative phosphorylation to glycolysis, resulting in the accumulation of lactate in the TME, which becomes acidic. [32,33]Moreover, HIF also promotes neovascularization, which refers to the formation of new blood vessels that irrigate the tumor, being associated with the vascular niche of OS.

Neovascularization can occur by the sprouting of endothelial cells present in pre-existing vessels, called angiogenesis, or by the recruitment and differentiation of endothelial precursor cells to be incorporated into new vessels, named vasculogenesis. Briefly, the release of HIF-1α by hypoxic tumor cells, as well as TGF-α and fibroblast growth factor (FGF)-2, promotes the upregulation of VEGF. [34] As a pro-angiogenic factor, VEGF will bind to its receptors in quiescent endothelial cells of the TME, promoting their sprouting, and activate MMPs and other proteolytic enzymes that degrade the ECM components, allowing the migration of endothelial precursor cells to the TME. The resulting tumor-associated blood vessels are usually immature and do not present junctions between endothelial cells, which facilitates the intravasation of tumor cells into the blood circulation. [35]Besides angiogenesis and vasculogenesis, another process called vasculogenic mimicry is observed in OS, in which tumor cells, independently of the vascular niche, form vascular-like microchannels. [36] In all cases, these newly formed structures allow the perfusion of the tumor and provide a route for intravasation, important for the metastatic spread of the tumor. [31,36]

As previously stated, ECM remodeling in OS is partly attributed to the degradation of its components by proteolytic enzymes, which are released by abnormally activated osteoclasts and in response to the hypoxic and acidic environment, both induced by tumor cells. This is a key mechanism for tumor cell invasion into the surrounding tissue. Simultaneously, there is an enhanced production of ECM by tumor cells, osteoblasts and stromal cells present in the TME. By secreting TGF-β and stromal cell-derived factor (SDF)-1, tumor cells recruit bone marrow (BM)-MSCs to the TME, where they differentiate into pro-tumorigenic stromal cells, including cancer-associated fibroblasts (CAF), and secrete growth factors and ECM components, such as collagen, fibronectin, laminin and proteoglycans. [14] As such, OS is generally characterized by a stiffer and denser stroma compared to healthy bone tissue, which hinders the anticancer function of immune cells, as they have more difficulty in penetrating the ECM and reaching the tumor site.[24]

The immune cell niche present in the OS-TME is mainly composed of tumor-associated macrophages (TAMs), which can be derived from macrophages present in the bone tissue or from circulating monocytes that are recruited by tumor cells. [37] Regardless of their origin, they may be M1-polarized, secreting pro-inflammatory signals that promote immune cell activation, or M2-polarized, secreting anti-inflammatory signals, thus decreasing immune cell proliferation. Both types can be observed in OS, but tumor cells usually induce a shift towards the presence of more M2-polarized TAMs in more aggressive and metastatic OS. [38] Cytotoxic lymphocytes such as T cells, which recognize foreign antigens, are also present within this niche. However, their activity is usually impaired, either by the induced immunosuppressive environment or downregulation of antigens by tumor cells. [31]

All these mechanisms allow the survival of tumor cells within the bone tissue and the establishment of metastases in other tissues. After migrating through the basement membrane of the nearby blood vessels, tumor cells enter the blood circulation and must evade the immune system, as well as resist *anoikis* , which is a particular type of apoptosis induced by the absence of cell-cell and cell-matrix adhesions.[39,40] The lungs are a frequent site of metastasis for OS, as the tumor cells that survive in the blood circulation become entrapped, given their larger diameter, in the alveolar capillaries, thus forming a secondary tumor. There, OS cells release TGF-β1, which promotes the transformation of lung fibroblasts into a cancer-associated phenotype, further allowing their survival.[41,42]

2.3 Relevance of 3D *in vitro* models

The development of preclinical cancer models is fundamental to understand tumorigenesis and tumor progression, discover potential new therapeutic targets, and assess the efficacy of novel anticancer drugs before their translation into clinical studies.[43,44,45] This is extremely important in OS research, since this is a very rare type of cancer with high mortality and resistance to chemotherapy. [45] As such, OS models should replicate the *in vivo* characteristics and behavior of the tumor, including its intra-heterogeneity, complex microenvironment and relevant cell-cell and cell-matrix interactions.[43]

Within *in vitro* models, two-dimensional (2D) models have been widely employed in OS research, due to

their reproducibility, simple implementation and inexpensive cost. [46] In fact, they have contributed to a great portion of the current understanding of OS, but they are, nonetheless, very simplistic models that do not accurately reflect the complexity of this cancer type: cells interact with each other in a different manner, compared to *in vivo* , as they grow as a homogeneous monolayer, rather than a three-dimensional (3D) structure, adopting a flattened morphology. Additionally, these models lack the presence of a surrounding matrix, which altogether induces a shift in the gene and protein expression of these cells, altering their response to chemotherapy and reducing the clinical relevance of these models. [47]

In vivo models are more physiologically relevant, as the tumor grows within a complex microenvironment, where the proper interactions between cells and with the surrounding matrix can be established.[19] These can be generated by using known carcinogens, genetically modified animals or by transplanting cancer cells into animals. [48] While genetically engineered models are important to study the role of different genes in OS, the most used *in vivo* OS models are transplantation models, as they have a high rate of tumor formation and require a short experimental period. Regarding xenotransplantation models, in which the tumor tissue is implanted into another animal species, a growing interest has been observed in patient-derived xenografts, as they preserve the heterogeneity and architecture of tumor tissues surgically removed from patients. [49] However, the drawbacks of animal models lie in ethical and welfare concerns, and in the difficulty in translating the preclinical outcomes between species,[50] as the tumor develops in an animal-derived microenvironment that does not exactly replicate the OS environment found in humans.

To address the shortcomings of *in vivo* and 2D *in vitro* OS models, 3D *in vitro* models have been recently used in OS research. [51] These are able to mimic not only the 3D macrostructure of the tumor, but its heterogeneity as well, since cells grow in multilayers that are differentially exposed to oxygen and nutrient gradients, much like in *in vivo* conditions.[46] Additionally, the cellular and non-cellular components of the bone TME can be incorporated in these models by employing co-culture methods and ECM-biomimetic scaffolds to encapsulate cells, respectively. [19,52] While the complexity of these models may vary, depending on the goal of the study, they ultimately offer a more accurate and clinically relevant representation of OS, as they can reproduce its key aspects without the need to use animals.

In general, 3D *in vitro* models of OS can be classified as scaffold-free or scaffold-based models, depending on whether a supporting matrix simulating the OS-TME is absent or present, respectively. The development of such models is a complex process that begins with selecting the proper OS cells to use, as cells from different tumors may present distinct characteristics, and the appropriate biomaterials to model the OS-TME. OS is commonly represented*in vitro* by immortalized cell lines established from primary tumors, including the MG-63, U2OS, HOS and Saos-2 cell lines, which present different phenotypes of OS, in terms of tumor initiation, growth and metastasis, [53] and have therefore been selected for different applications in OS-related research. For example, MG-63 cells are frequently used in 3D spheroid culture due to their high ability to form colonies, [54,55,56] while U2OS cells are preferred for invasion and migration studies.[57,58,59] More complex models may incorporate co-culture systems to introduce other cell types present in the OS-TME, as well as biomimetic cues.

3. Biomaterials used to model the OS-TME

In order to accurately mimic the complexity of OS *in vitro* , the biomaterials employed in 3D *in vitro* models should present similar features of the OS-TME. These include a similar composition of the tumor ECM and adequate mechanical and structural properties, including stiffness. In addition to biocompatibility, these biomaterial scaffolds should also have a suitable porosity, as this dictates the efficient diffusion of nutrients and migration of cells.[60]

With these requirements in mind, many biomaterials have been used in OS scaffold-based models, either of natural or synthetic origin. Natural-origin materials closely resemble the composition of biological tissues, including bone and OS, and typically contain cell adhesion motifs, providing an environment that is favorable

for cell proliferation. [52] However, compared with synthetic polymers, whose mechanical and structural properties can be easily tuned, they often lack stability and exhibit poorer mechanical properties. [51] Additionally, synthetic materials present minimal batch-to-batch variability, which allows the development of scaffolds with great reproducibility. Still, they lack cell adhesion motifs and have an impaired bioactivity, usually requiring further functionalization. To address the issues of both types of materials, combinations of natural and synthetic materials have been explored for 3D OS scaffolds. [61,62,63]

3.1 Natural Biomaterials

Matrigel : Matrigel® is a commercially available reconstituted basement membrane matrix, extracted from murine Engelbreth-Holm-Swarm (EHS) sarcoma. [64] It has been widely used to create 3D scaffolds for *in vitro* tumor models, due to its complex composition of ECM proteins (e.g., laminin, collagen type IV and proteoglycans) and growth factors (e.g., TGF-β) and its spontaneous polymerization at 37 ºC. [51,64]Particularly in OS research, Matrigel has been employed in the generation of 3D OS-CSC models, due to its tumorigenic origin[60,64], as well as in 3D invasion assays.[65,66,67] However, there are several drawbacks to using this protein-rich mixture, including batch-to-batch variability, poor mechanical properties and the presence of animal-derived growth factors, which may alter how tumor cells react to chemotherapeutic drugs. [14] Therefore, pure 3D Matrigel scaffolds for drug screening OS models are rare. Instead, a common approach is to use Matrigel in combination with other materials, including collagen.[68,69]

Collagen: As the major constituent of the OS-TME, collagen type I is an attractive material to produce 3D *in vitro* OS scaffolds.[14,51] It is composed of polypeptide chains that self-assemble into a triple helix structure, which then organize themselves into fibrils and eventually larger fibers. This occurs spontaneously under physiological conditions, namely neutral pH and 37 ºC. [52] As such, a neutralizing buffer is usually used to neutralize the acidic pH of the solubilized collagen solution, which is then incubated at 37 ºC. Collagen is usually obtained from the tendon of rat tails and, as an ECM component, it possesses cell adhesive domains, including the arginine-glycine-aspartate (RGD) peptide, and degradable sites recognized by enzymes, which allow cell proliferation and matrix degradation, respectively. [70] For 3D*in vitro* OS models, collagen has been used for drug screening and cell migration studies [67,71,72,73] and has been combined with other materials, including hydroxyapatite (HAp) nanoparticles [74], in order to enhance its stiffness or bioactivity. [52]

Gelatin: Gelatin is obtained from the irreversible denaturation of collagen, through heat or enzymatic processes, which destroy the triple helical structure and produce random coils.[75] Like collagen, gelatin has cell adhesive domains and degradable sites, but it is physically crosslinked below physiological temperatures, in a reversible way.[76] This property has been explored in sacrificial micromolding techniques to produce 3D cellular aggregates: cells were deposited onto microwells patterned in gelatin layers and the resulting aggregates were released by melting the gelatin layer at 37 ºC. [77] Nonetheless, due to its poor mechanical properties and reversible crosslinking, gelatin is commonly used in 3D*in vitro* OS models in a modified way[19,78,79] and/or in combination with other materials. [61,80,81] Modification of gelatin commonly refers to the addition of functional groups, namely methacrylate (MA) groups. These are photocrosslinked by visible or UV light, in the presence of photoinitiators, such as Lithium phenyl-2,4,6-trimethylbenzoylphosphinate (LAP). The resulting gelatin methacryloyl (GelMA) can thus be irreversibly crosslinked in a controlled way, by adjusting the time of exposure, the degree of substitution and the photoinitiator concentration, allowing the production of structures with different stiffness.[82]

Silk Fibroin: Silk fibroin is one of the proteins that compose silk, which is a natural polymer usually extracted from cocoons of*Bombyx mori* silkworms. [83] It has good mechanical properties, supports cell adhesion and can be manipulated to produce different scaffold morphologies, including porous meshes, hydrogels and microparticles. [84] As such, it has been fairly used for bone tissue engineering,[85,86,87] while its use in 3D *in vitro* OS models has only recently been reported. [88,89,90]

Alginate: Alginate is a polysaccharide obtained from brown seaweed and is an interesting biomaterial for 3D OS models due to its similarities to the glycosaminoglycans (GAGs) found in the bone TME.[91,92] In

the presence of divalent cations, such as Ca^{2+} and Mg^{2+}, the guluronate residues of alginate can be easily crosslinked, through their carboxyl groups, resulting in a negatively charged 3D structure.[93] In OS research, alginate has been mostly exploited to create beads in which 3D OS cellular aggregates can be formed. [94,95] However, the absence of cell adhesion motifs has motivated its combination with other biomaterials that have adhesion proteins, such as gelatin.[96,97]

Chitosan: This polysaccharide is usually extracted from the exoskeletons of crustaceans, but it can also be found in fungi and insets. [98] Chitosan has a similar structure to GAGs, like alginate, and promotes cell adhesion and proliferation, having been used in bone tissue engineering. [99]More recently, a few chitosan scaffolds for culturing OS cells have been reported, typically in combination with other materials, such as alginate [100] and HAp[101], in order to enhance its poor mechanical properties. [102]

Decellularized Extracellular Matrix : The ECM produced by cells present in the bone TME has been used to make 3D scaffolds for bone regeneration and *in vitro* tumor models, due to its structural and compositional biomimicry of the bone ECM.[103,104] Decellularized extracellular matrices (dECM) are obtained through the decellularization of *in vitro*cell cultures or native tissues, which consists of removing their cellular components, giving rise to cell-derived or tissue-derived dECMs, respectively. [105,106] The use of tissue-derived dECM captures the native complexity of tissues, including their microarchitecture, but presents challenges. These include the need to optimize the decellularization protocols, which may span from 30 min to 96 h, and the inherent batch-to-batch and tissue variability. In contrast, cell-derived dECM can be easily retrieved, offering high reproducibility and the possibility to manipulate the ECM composition and deposition rates. [104] While cell-derived dECM may lack *in vivo* complexity, compared to tissue-derived dECM, it is recently becoming more used by researchers due to its advantages. Depending on the tissue source or cell types chosen, dECM may be composed of specific proteins mixtures, including collagen, GAGs, proteoglycans and growth factors. [52] The decellularization process should be neither too intense, as to destroy the tissue microstructure, which could inhibit cell adhesion and migration, neither too mild, since the presence of the original cells may inhibit the growth of the subsequent inoculated cells.[107] Thus, the decellularization agents should be carefully chosen to retrieve the matrix efficiently and these commonly include chemical surfactants, such as sodium dodecyl sulphate (SDS), sodium deoxycholate (SDC) and Triton X-100, which can be further conjugated with enzymatic and acid/basic agents, such as trypsin and ammonium hydroxide, respectively. [108] Even though dECM derived from cultured osteoblasts/OS cells retains the complex composition of the bone TME, including its proteins, signaling cues and proper cell adhesion and degradation motifs,[109] which are necessary for cell proliferation, only a few 3D *in vitro* OS models have been developed using this biomaterial. [110,111]

3.2 Synthetic Materials

Poly(ethylene) Glycol (PEG): PEG is a bioinert and nondegradable polymer synthesized by the polymerization of ethylene oxide. PEG's inertness arises from its hydrophilicity, which prevents protein adsorption and, consequently, cell adhesion.[112] To control its crosslinking process, a common modification of PEG is the addition of acrylate groups, forming PEG-diacrylate (PEGDA), which can be crosslinked by UV exposure in the presence of photoinitiators. [113] Moreover, the mechanical properties of PEGDA, including its stiffness, can be carefully optimized by changing its crosslinking degree[114] and, to allow cell adhesion, PEG chains can also be functionalized with cell-binding peptides, such as the RGD peptide. [112] Overall, PEGDA has been extensively used in bone and cartilage tissue engineering and, more recently, in 3D OS models, either alone [115] or in combination with other biomaterials, such as GelMA [79] and hydroxyapatite. [116]

Πολψ(ε-ἁπρολαςτονε) (ΠˆΛ): PCL is another popular synthetic polymer for 3D *in vitro* tumor models. It is prepared by the polymerization of ε-caprolactone and, due to its synthetic origin, it is commonly functionalized with cell-adhesive motifs to ensure cell proliferation. [117] Under physiological conditions, PCL develops a rubbery-like conformation that offers high toughness, strength, and elasticity. [118] In addition to its tunable mechanical properties, PCL can be easily integrated with other materials. As such, PCL fiber meshes, blended or not with other biomaterials, including gelatin,[61,80] alginate [62] and cell-derived dECM,

[63] have been used as biomimetic scaffolds for 3D *in vitro* OS and Erwing sarcoma models.

Poly(vinyl alcohol) (PVA) : PVA, derived from the hydrolysis of poly(vinyl acetate), is a water-soluble synthetic material known for its non-toxicity, biodegradability and good mechanical strength and flexibility [119,120]. Its drawbacks include rapid dissolution in water and bioinertness, requiring further modification for cell adhesion. [121] In the context of 3D*in vitro* models of OS, PVA has been used to create electrospun nanofibers in combination with gelatin [81] and silk fibroin [87], given its sufficient electroconductivity [122].

4. 3D bioengineered *in vitro* OS models

Many different 3D *in vitro* strategies with varying degrees of complexity have been explored to develop OS models, which include the use of multicellular tumor spheroids, ECM-mimetic biomaterials to encapsulate tumor cells and, more recently, microfluidics and 3D bioprinting.

4.1 Scaffold-free spheroids

Multicellular tumor spheroids are spherical aggregates of tumor cells and are currently the major 3D *in vitro* platform used in cancer research as they present similar features to *in vivo* tumors. These include the presence of a heterogeneous tumor population, as well as similar oxygen and nutrient gradients, necrotic regions and drug penetration rates. [123] Tumor spheroids were introduced in the 1970s and, since then, have elucidated many aspects of tumor biology and drug resistance for different cancer types, including OS. [124,125]

The spheroid tumor model presents an intermediate complexity between the conventional 2D monolayer cultures and *in vivo* tumors, having three distinct zones within their spherical shape.[126] These consist of an outer layer of rapid proliferating cells, followed by an intermediate layer with quiescent cells and, lastly, a central core where cells are under necrosis.[125] This cellular and radial variation can be explained by the oxygen gradient established within the tumor spheroid:[127] while oxygen can be diffused to the outer cells, it cannot reach the center of the spheroid and, as such, these inner cells revert to the anaerobic metabolism, producing lactate and therefore lowering the pH. Due to this hypoxic and acidic environment, the cells present in the inner regions become stagnant in the G0-G1 phase of the cell cycle, in a non-proliferative and dormant state, but still produce growth factors involved in tumorigenesis. As the tumor grows, the fraction of proliferative cells, in the outer layers, decreases, while the fraction of the non-proliferative cells in the inner regions increases. At the core, cells eventually die, forming a necrotic center region. [126] Most commonly, this three-layered structure is observed in spheroids with a diameter higher than 250 μm, including those obtained from OS cells.[128]

Spheroids are formed *in vitro* without the use of a supporting scaffold and in a spontaneous manner, when cells interact minimally with surfaces and, instead, self-aggregate. [129]Several techniques have been developed to create the conditions necessary to generate spheroids, and these mainly differ in the way cells are prevented from interacting with the surface.[127,130] For example, with the hanging drop method, cells are suspended in small drops of culture medium that are deposited in glass coverslips; when these are inverted, gravity forces cells to self-aggregate at the bottom of the drop.[131] The continuous stirring in spinner flasks has also been exploited to form spheroids, as cells are kept in suspension, which promotes cell-cell adhesion.[132] Another strategy is to seed cells on non-adhesive surfaces, such as superhydrophobic or coated surfaces, with the so-called liquid overlay technique. [133] More recently, the use of microfluidics has also been explored to culture spheroids, where cells circulate through microchannels, suspended in culture media, and accumulate in microchambers. There are also commercially available products, such as Aggrewell™plates (STEMCELL Technologies, Inc.) and Perfecta3D™hanging drop plates (3D Biomatrix, Inc.), for the generation of spheroids in a high throughput manner. [130]

Several studies have used OS spheroids to evaluate the cytotoxicity of the chemotherapeutics included in

standard OS treatment, in 3D conditions. For example, early in 1980, West et al. [134] accessed the penetration of methotrexate into HOS cell aggregates. The drug affected only a small portion of the spheroids' proliferative cell population which, combined with the observed limited penetration when compared to 2D monocultures, partly explained its limited clinical success.[134] Regarding doxorubicin, Arai et al.[135] observed that tumor spheroids from multiple OS cell lines, including HOS and MG63 cells, had an increased resistance to the drug, in comparison to monolayer cultures. Additionally, cathepsin D, which had previously been linked to chemoresistance of other cancer types, was found to be upregulated in spheroid culture, indicating that this protein may be involved in the molecular mechanisms of OS chemoresistance. [135] These findings were later corroborated by Rimann et al. [136], which produced spheroids from Saos-2, HOS and MG-63 cell lines, using the hanging drop method. The spheroids presented different sizes, morphologies and chemoresistance, depending on the cell source, and showed increased doxorubicin and cisplatin IC_{50} values, in comparison to their 2D counterparts. The highest cytotoxicity was observed in Saos-2 spheroids, which had the highest percentage of proliferative cells among all spheroid types, observation that is consistent with the action mechanism of these drugs.[136] In another study conducted by Baek et al.,[128] the effects of doxorubicin on the viability and integrity of U2OS spheroids were studied in a real time-manner. Doxorubicin cytotoxicity was only observed one day after treatment, with spheroids presenting a decreasing size and ATP production with time, in a concentration-dependent manner. Three days post-treatment, cellular activities and ATP production were arrested, which suggests that doxorubicin might require internalization into the cytosol, via endocytosis, to be effective. [128] The same research group performed a similar study with cisplatin and equivalent results were obtained. [137]

The potential of novel compounds to serve as anticancer drugs for OS has also been assessed with spheroid models of OS. An example of such compounds is VOChrys (oxidovanadium(IV) complex with chrysin (V)), which is composed of vanadium, a trace element that accumulates in bone after it is absorbed by the organism, and the flavonoid chrysin, which was shown to have antitumor activity. [138] As such, León et al. [138] studied the antitumor activity of VOChrys and found that the compound was able to decrease the viability of MG-63 spheroids, reducing their metabolic activity by 35% and their volume when compared with non-treated spheroids, making this a promising new anticancer drug for OS. [138] In the same line of action, novel targets of OS have also been investigated in these 3D platforms, namely the nuclear NAD synthesis enzyme (NMNT1), which had been found to be overexpressed after U2OS cells were treated with cisplatin. This enzyme participates in the synthesis of nuclear NAD+ which is a substrate for the Poly [ADP-ribose] polymerase 1 (PARP1) responsible for recognizing and repairing DNA damage.[139] In this regard, Kiss et al.[139] generated NMNT1-inactivated U2OS spheroids, which showed lower levels of NAD+, potentially impairing the DNA damage recognition by PARP1. After treatment with cisplatin, spheroids showed a great reduction in size, confirming the potential role of NMNT1 as a target for future OS therapeutic approaches. [139]Other novel strategies for OS treatment have been evaluated in 3D spheroid cultures. In a recent work, Marshall et. al[54] studied the efficacy of combining chemotherapy, radiopharmaceutical therapy and nanotechnology in MG-63 spheroids, by using nanoparticles loaded with doxorubicin and radionuclide $Na^{131}I$ and labelled with the epidermal growth factor receptor (EGFR) antibody. The labelled nanoparticles selectively bound to MG-63 cells, showing increased cytotoxicity compared with unlabeled nanoparticles. The combination of doxorubicin and $Na^{131}I$ proved more cytotoxic than doxorubicin alone, generating free radicals and impairing DNA repair. Overall, two main conclusions were reached: i) the use of labelled nanoparticles can be exploited to deliver a higher effective therapeutic dose to the cells and ii) the combination of chemotherapeutic drugs and radionuclides seems to be more effective than monotherapy. [54]

Many aspects of OS tumorigenesis have been studied with spheroid-based models as well, including the effect of hypoxia on cell adhesion. Indovina et al. [56] simulated the hypoxic environment of *in vivo* tumors by incubating MG-63 spheroids with low oxygen concentration (less than 1%) and exposing them to chemicals that activate hypoxia-dependent pathways. The authors concluded that, besides promoting angiogenesis and metabolic reprogramming, hypoxia also influences OS adhesion – which is crucial for tumor cells to invade the surrounding tissues – since spheroids grown under hypoxia showed higher adherence to collagen/fibronectin-coated plates and fibroblast monolayers, along with the loss of their spherical shape.[56]

Tumor neovascularization has also been simulated in OS spheroid models due to its importance in tumor biology and drug delivery. This is often done by co-culturing tumor cells with endothelial cells, which have a key role in neovascularization. For instance, Chaddad et al. [140] developed a vascularized 3D OS model by depositing MG-63 spheroids on a 2D monolayer of human umbilical vein endothelial cells (HUVECs). The 3D OS environment enhanced the production of angiogenic factors, such as VEGF, in comparison to 2D MG-63 monolayers, which helped to attract HUVECs towards the spheroids. Subsequently, the HUVECs formed tubule-like structures that self-organized into capillary networks (10-25 μm in diameter), thus successfully mimicking *in vivo* vessel-like structures (**Figure 2** A). [140]

Within the heterogeneous cell population of OS, the presence of CSCs has been confirmed with the sphere-forming assay, which involves culturing cancer cells in stressful growth conditions to only promote the proliferation of those with stem cell-like self-renew properties. Using this method to produce CSCs spheroids from the MNNG/HOS cell line, Martin-Neves et al. [16] demonstrated the need to develop OS-CSC-targeted therapies, as the spheroids presented higher resistance to common cytotoxic drugs and radiation when compared with the heterogeneous population of the original cell line, along with decreased production of free radicals and increased expression of drug efflux transporters. [16] In that sense, Guo et al. [141] found that miRNA-335, a non-coding RNA that had been associated with tumor progression in other cancer types, was less expressed in OS-CSCs spheroids and could be useful in OS treatment, as miRNA-335 pre-treatment showed an increased sensitivity of spheroids to cisplatin. [141] Another common approach to isolate CSCs from the rest of the cancer cells is to perform magnetic-activated cell sorting (MACS), using stem cell surface markers, such as CD133. Ozturk et al. [142] was able to create spheroids from both $CD133^+$ (CSC) and $CD133^-$ (non-CSC) subpopulations of the Saos-2 cell line, which contradicted previous findings linking the spheroid-forming ability of cancer cells with stem cell properties.[143] This suggests a potential transformation of non-tumorigenic ($CD133^-$) cells towards a tumorigenic phenotype, known as the "dynamic cancer stem cell model", possibly induced by the 3D culture system. Nonetheless, $CD133^+$spheroids exhibited the highest cell viability and maintained their pluripotency. [142] Rainusso et al.[15] employed fluorescence-activated cell sorting (FACS) to isolate the CSC subpopulation of several OS cell lines, including MNNG/HOS, 143B, Saos-2 and MG-63. Using the long-term label retention dye PKH26, slowly dividing (quiescent) CSCs exhibited high fluorescence, whereas rapidly dividing non-CSCs displayed reduced fluorescent levels. In contrast to the entire tumor population, the isolated CSC subpopulations showed superior efficacy in forming 3D*in vitro* sarcospheres and inducing tumors in immunocompromised mice, along with an upregulation of genes related to migration.[15]

In order to mimic the crosstalk between OS cells and stromal cells that happens *in vivo* , heterotypic spheroids, composed of two or more cell types, have also been developed, usually employing MSCs. Using OS/MSC heterotypic spheroids, Cortini et al. [144]demonstrated that most ECM proteins are synthesized by the mesenchymal stroma of OS, since the presence of MSCs enhanced ECM production in the spheroids. The deposition of collagen by MSCs, regulated by IL-6, promoted an increased resistance to doxorubicin, suggesting the importance of ECM-targeting strategies for OS treatment and the necessity of modeling the OS stroma in drug screening.[144] Freeman et al. [145]modelled earlier and later stages of OS using heterotypic spheroids with different ratios of MSCs to Saos-2, namely 3:1 and 1:3, respectively. Compared with homotypic spheroids, both co-culture spheroids exhibited increased diameter, higher expression of OS prognostic markers and reduced tumor growth post-doxorubicin treatment. The late-stage model presented limited upregulation of doxorubicin-mediated apoptotic genes, compared to the early-stage model, thus recapitulating the higher resistance of late-stage *in vivo* OS to chemotherapeutic drugs (**Figure 2** B). [145] In another study led by Lenna et al. [146], different MG-63:MSC ratios were used to produce heterotypic spheroids and evaluate the efficacy of a new photodynamic therapeutic strategy. Nanoparticles functionalized with photosensitizers were delivered by MSCs to OS cells, resulting in decreased cell viability in all spheroids after photoactivation. The effect was less pronounced in spheroids with higher MG-63:MSC ratio, due to MG-63 cell outgrowth, which confined MSCs to the inner spheroid regions. As such, the tumor dimensions and the number of loaded MSCs that can reach the tumor site will dictate the *in vivo* efficacy of this strategy to kill OS cells. [146]

The aforementioned studies highlight the benefits of using 3D scaffold-free spheroids to model OS, as they can mimic several *in vivo* features of the tumor, including its 3D macrostructure, the presence of a necrotic core and the crosstalk between tumor and stromal cells by using heterotypic cultures. However, unlike scaffold-based models, the spheroid model does not recapitulate the complex extracellular matrix that surrounds the tumor.

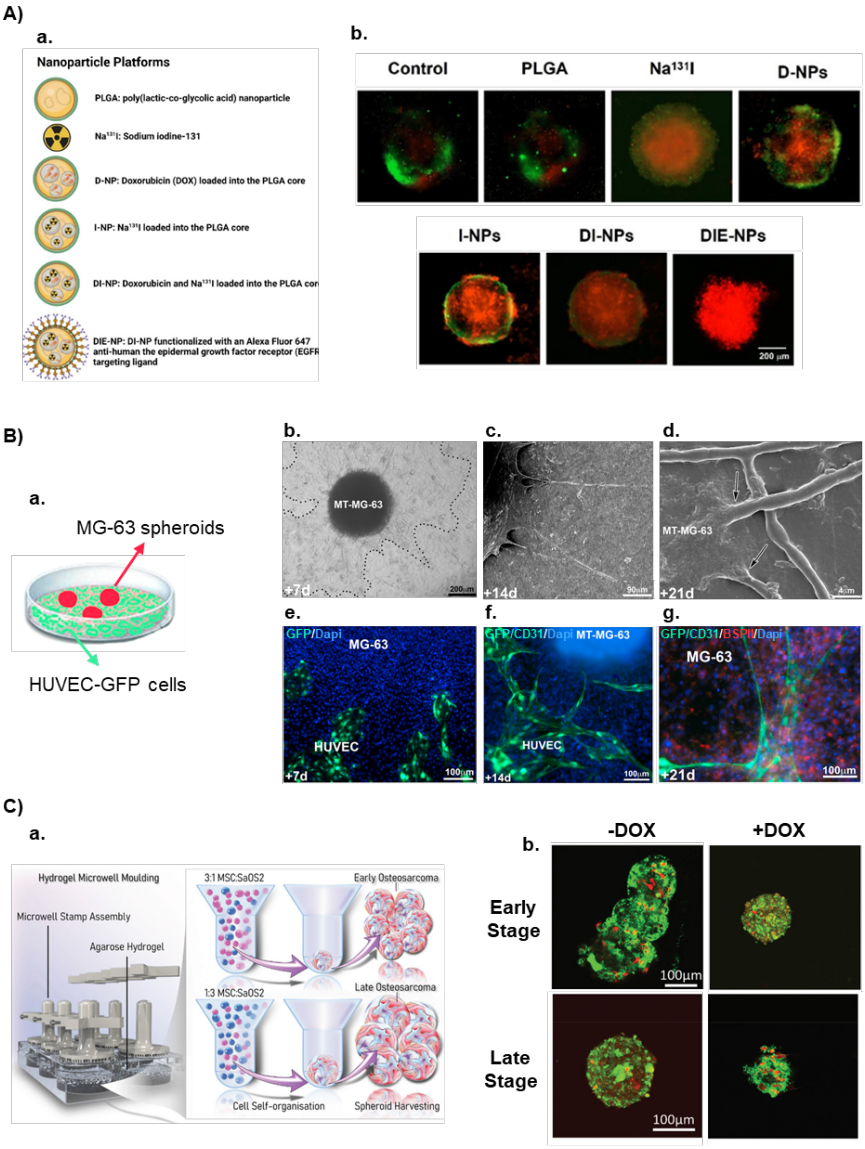

Figure 2. (A) Combination of chemotherapy, radiotherapy and nanotechnology as a novel treatment strategy for OS.[54] (a) Schematics of the different nanotherapeutic platforms used. (b) Live/dead imaging of MG-63 spheroids treated with control, PLGA nanoparticles (NPs), Na131I, D-NPs, I-NPs, DI-NPs and DIE-NPs. Reproduced with permission.[54] Copyright 2022, MDPI. (B) Simulation of OS vascularization through the combination of MG-63 spheroids and 2D monolayers of HUVECs. [140] (a) Graphical representation of the OS tumor model developed by Chaddad et al.[140]. (b) Optical microscopy and (c-d) scanning electron microscopy images of MG-63 spheroids in culture with HUVECs: (b) after 7 days, MG-63 cells migrated and formed a migration front; (c) After 14 and (d) 21 days, HUVECs formed tubule-like structures, which

appeared to enter the spheroid (arrows). (e-g) Immunofluorescence for GFP, CD31 and BSPII of combined cultures. Reproduced with permission.[140] Copyright 2017, Elsevier (C) Modeling of different stages of OS using heterotypic spheroids composed of Saos2 cells and MSCs. [145] (a) Schematics of the conditions used to develop early- and late-stage OS spheroids. (b) Live/dead imaging of early and late-stage tumor spheroids with and without doxorubicin treatment. Reproduced with permission.[145] Copyright 2021, John Wiley and Sons.

Table 1. Summary of three-dimensional *in vitro*scaffold-free spheroid models developed for OS research.

OS cell type	Co-culture cells	Therapeutic treatment	Findings	Ref
HOS	–	Methotrexate	Methotrexate had a limited penetration in spheroids with diameters exceeding 250 μm.	[134]
Saos-2, SJSA-1, KHOS/NP, HOS, HuO9, MG-63, MNNG-HOS, 143B, HS-Os-1, NOs-1, Nos-10	–	Doxorubicin	OS spheroids showed an increased chemoresistance, compared to 2D cultures. The protein cathepsin D was found to be upregulated in spheroid culture.	[135]
Saos-2, HOS, MG-63 and OS cells from patients	–	Doxorubicin, cisplatin, taurolidine, taxol, permetrexed,	The size and morphology of the spheroids depended on the cell line. IC_{50} values were higher in 3D culture than in 2D monolayer.	[136]
U2OS	–	Doxorubicin	Doxorubicin needs to be endocytosed to exert its antitumor activity. Higher IC_{50} values were obtained for this 3D culture system.	[128]

OS cell type	Co-culture cells	Therapeutic treatment	Findings	Ref
MG-63	–	VOChrys	Treatment with VOChrys led to a decrease in cell viability and altered shape and volume of spheroids. Thus, this compound is a potential candidate for anticancer treatment.	[138]
U2OS	–	Cisplatin	Spheroids with inactivation of NMT1 showed a significant size reduction after cisplatin treatment.	[139]
MG-63	–	Doxorubicin, Radionuclide $Na^{131}I$ and Nanoparticles	The combination of chemotherapeutics, radiopharmaceutical therapy and nanotechnology resulted in a higher cytotoxicity and a significant reduction of the G0/G1 spheroid population.	[54]
MG-63	–	–	Spheroids cultured under hypoxic conditions showed an increased adhesion to collagen and fibronectin coated plates.	[56]

OS cell type	Co-culture cells	Therapeutic treatment	Findings	Ref
MG-63	–	–	Tumor spheroids were cultured on top of a 2D HUVEC monolayer to induce angiogenesis. Tubule-like structures were formed by HUVECs, which invaded the tumor spheroids.	[140]
MNGG/HOS	–	Doxorubicin, cisplatin, methotrexate, ionizing radiation	CSC spheroids were produced by culturing the tumor cells under stressful conditions and showed higher resistance to cytotoxic drugs and radiation.	[16]
MNNG/HOS, 143B, Saos-2, MG-64	–	–	The CSC subpopulation of OS cells, isolated with FACS, showed a higher efficacy in producing 3D sarcospheres and an upregulation of migration-related genes.	[15]
MG-63, U2OS, 143B		Anti-miRNA-335, Cisplatin	Pre-treatment with miRNA-335 increased the sensitivity of OS-CSC spheroids to cisplatin.	[141]

OS cell type	Co-culture cells	Therapeutic treatment	Findings	Ref
Saos-2	–	–	CSC spheroids were generated with the $CD133^+$ subpopulation of Saos-2 cells and exhibited a higher viability, compared with non-CSC ($CD133^-$) and Saos-2 spheroids.	[142]
MG-63	MSC	Doxorubicin	ECM proteins were mostly secreted by MSCs and IL-6 was found to regulate the collagen deposition by MSCs, which increased the resistance of MG-63 cells to doxorubicin.	[144]
Saos-2	MSC	Doxorubicin	Early and late-stage models of OS were developed using different OS:MSCs ratios. The late-stage model showed a higher resistance to doxorubicin.	[145]
MG-63	MSC	Nanoparticles functionalized with photosensitizers	MSCs delivered the nanoparticles to MG-63 cells, resulting in decreased cell viability after photoactivation.	[146]

4.2 Scaffold-based models

In vitro scaffold-based models of OS have employed a variety of material settings, namely hydrogels, spongy-like scaffolds, electrospun fiber meshes and, more recently, microfluidic and 3D bioprinted constructs. [51] Additionally, several scaffolds for bone tissue engineering have been developed with OS cell lines, which, despite not exploring drug resistance mechanisms and novel anticancer drugs, have also provided valuable information on OS cell proliferation in different types of biomaterials.

4.2.1 Hydrogel-based models

Within the scope of scaffolds used for 3D culture of OS cells, hydrogels have been the most widely used. These are polymeric networks generally synthesized by physical or chemical crosslinking, presenting high water content, tunable biophysical and biochemical properties and variable stiffness between 1 and 150 kPa. [52,147] As such, they are able to encapsulate tumor cells and acquire different architectures, porosity, shapes and mechanical cues.[148] Sponges, or spongy-like hydrogels, present a higher pore size and larger surface area compared with simpler hydrogels, which improves cell adhesion. [51,147]They are produced from hydrogel precursors, which are frozen and then lyophilized, resulting in a porous matrix. [147]

The activation of several pathways related to cancer biology has been studied in OS, using these scaffold types. For example, Baranski et al. [68]used a collagen/Matrigel hydrogel scaffold to investigate the role of the MEK (mitogen-activated protein kinase) signaling pathway in 3D environment in several OS cell lines. This pathway, activated by the mutation/overexpression of receptor tyrosine kinases (RTKs), often hyperactive in cancers, leads to ERK (extracellular-signal-regulated kinase) phosphorylation by MEK. Half of the cell lines showed high ERK activation, which was reduced after treatment with MEK inhibitors, resulting in decreased cell viability. As such, these 3D culture systems validated the efficacy of MEK inhibition for treatment of OS with high ERK activity, which had already been demonstrated in 2D conditions.[68] The role of the secreted frizzled-related protein 2 (sFRP2), an extracellular signaling molecule involved in the regulation of the Wnt pathway that is usually overexpressed in metastatic cancer, was also studied in OS. Using a 3D Matrigel scaffold, Techavichit et al. [65] found that sFRP2 promoted the migration and invasion of HOS cells *in vitro* . Conversely, Orosco et al. [66] discovered that syndecan-2, a transmembrane heparan sulphate proteoglycan, has a protective antitumor role in OS. MG-63 and U2OS cells, encapsulated in Matrigel hydrogels, exhibited lower syndecan-2 levels compared to osteoblasts. Overexpressing syndecan-2 reduced cell migration and increased doxorubicin sensitivity. The authors hypothesized that decreased syndecan-2 expression in OS cells may sustain an undifferentiated phenotype, disrupting apoptosis-related pathways and enhancing chemoresistance. Consequently, syndecan-2 emerged as a potential new target to improve chemotherapy efficacy. [66]

In another study, Fallica et al. [72] produced scaffolds with different stiffness for U2OS encapsulation, using varying collagen concentrations. Compared with 2D monolayers, the 3D biomimetic environment contributed to reduced cell proliferation, migration rates and activation of the PI3K (phosphatidylinositol 3-kinase) pathway, commonly activated in cancers for cell growth and migration. Interestingly, stiffer scaffolds with similar PI3K activation showed an increased resistance of U2OS cells to PI3K inhibitors, possibly due to the activation of an alternate survival pathway, emphasizing the ECM's role in regulating the behavior and drug resistance of OS cells.[72] Another important protein involved in tumor progression is the vascular endothelial-cadherin (VE-cadherin), which is expressed in both endothelial and OS cells. Using siRNA technology to inhibit its expression in MG-63 cells cultured in collagen and Matrigel scaffolds, Zhang et al. [149] observed a reduction in angiogenic sprouting and in the formation of endothelial-like networks. The authors concluded that VE-cadherin might be involved in the transdifferentiation of OS cells into endothelial-like cells, promoting the vasculogenic mimicry that is observed in OS.[149]

The interactions of OS cells with collagen were accessed by Elenjord et al., [150] using 3D fibrillar scaffolds and 2D layers of monomeric collagen. OS cells adhering to 3D collagen fibers showed a more rounded morphology and decreased production of active MMP-2, compared with cells attached to monomeric collagen. This underscores the impact of the bone TME structure on MMP expression in OS cells, potentially influencing the invasive and metastatic spread of the tumor. [150] Jiang et al.[151] investigated the effect of ECM elasticity and adherence on the proliferation of MG-63 cells encapsulated in collagen, Matrigel, agarose or alginate hydrogels. On 2D films, cells were sensitive to ECM adherence, whereas, on 3D scaffolds, their sensitivity shifted toward ECM elasticity. The results suggest that 2D cultured cells are mainly influenced by ECM bioactivity, adopting unnatural characteristics, such as a flattened morphology, increased sensitivity to apoptosis and lower expression of genes related to tumor malignancy. However, their malignant phenotype can be recovered by culturing cells in 3D platforms that mimic the ECM of natural OS, being mainly

regulated by ECM elasticity. [151]

Tan et al. [89] demonstrated that the 3D architecture of the surrounding matrix might affect the morphology of OS cells and the expression of factors involved in their malignant potential. The authors fabricated 3D *in vitro* porous silk constructs in which 143B cells were seeded. Compared with the 2D culture system, cells cultured in 3D presented a spindle-like morphology and a higher expression of angiogenic markers, such as HIF-1α and VEGF-A, thus mimicking the *in vivo* OS physiology. [89]Later, by using GelMA hydrogels with different stiffness, Sawyer et al.[152] observed that OS cell function, viability and morphology were not only influenced by the 3D architecture of the ECM, but also by its stiffness. Softer and more porous scaffolds promoted higher cell viability and the formation of large cell clusters within the hydrogel, while stiffer hydrogels showed a predominant cell distribution along their periphery, suggesting that cells migrated due to the lower nutrient diffusion caused by the lower porosity of the scaffolds. [152]

Using PEGDA hydrogels, Jabbari et al. [115] also investigated how matrix stiffness affected OS cell growth. By varying the PEGDA concentration, hydrogels with different stiffness were developed, in which U2OS cells were encapsulated. A matrix stiffness of 55 kPa was found to enhance the expression of epithelial-mesenchymal transition (EMT) markers in cells, resulting in the enrichment of CSCs. This finding suggests that the CSC subpopulation of OS resides in a niche with specific matrix stiffness conducive to optimal interaction with the surrounding matrix. [115] The 3D spatial configuration of OS cells also confers chemoresistance, as reported by Tan et al. [90] Using another 3D silk fibroin model, encapsulated U2OS and Saos-2 cells exhibited G1 cell cycle arrest and reduced proliferation. Upon reseeding in 2D monolayers, cells reentered the cell cycle, displaying increased sensitivity to doxorubicin, compared to 3D cultured cells. In contrast, cisplatin showed no significant differences between the two conditions, aligning with its distinct work of action. The chemoresistance of OS cells is, thus, largely dependent on the characteristics of the surrounding matrix, which affect their viability and proliferation.[90]

The combination of chemotherapy and photothermal therapy as a possible treatment for OS was studied by Yang et al. [153]using a chitosan scaffold incorporating ferrite ($SrFe_{12}O_9$) particles and calcium silicate ($CaSiO_3$) microspheres, loaded with chemotherapeutic drugs. MG-63 cells exhibited high cell viability and proliferation, which significantly decreased upon doxorubicin treatment and near infrared radiation (NIR) exposure. Exposure to radiation, therefore, allowed a faster and more localized release of doxorubicin, making this a promising strategy to increase the clinical efficacy of chemotherapeutics for OS (**Figure 3** A).[153] Cold atmospheric plasma (CAP) has also emerged as a promising anticancer treatment, due to its composition of reactive oxygen and nitrogen species (RONS). When applied to *in vitro* cell cultures or superficial tumor tissues, CAP exploits the weaker antioxidant mechanisms of cancer cells compared to normal cells, inducing apoptosis. [154] While some studies had demonstrated antitumor effects on OS cells in 2D cultures and 3D models,[155] the impact of CAP within a relevant 3D OS-TME remained explored. Tornin et al. [74]addressed this gap and created a 3D spongy-like scaffold composed of collagen and HAp particles. Exposure to varying doses of plasma-activated solutions (PAR) revealed that only the highest dose was cytotoxic in the 3D model, contrary to 2D conditions. The 3D environment protected cells from PAR-induced apoptosis by scavenging ROS and upregulating CSC-related genes. The authors concluded that CAP treatment might not be advantageous in 3D conditions, as it enriched the CSC subpopulation of the tumor, implying potential limitations for CAP as an OS treatment. [74]

Recently, core-shell alginate-gelatin capsules have been reported by Ke et al. [96] as a novel 3D platform for MG-63*in vitro* culture. Gelatin was used for the core region, to promote cell adhesion and proliferation, while alginate was chosen as the shell polymer to enhance the stability of the capsules and protect the inner regions. MG-63 cells encapsulated in the gelatin core formed clusters, presenting increased cell viability and expression of osteogenic markers when compared with 2D monolayer cultures.[96] Kundu et al. [88] used gellan gum(GG)-silk fibroin(SF) hydrogels with two compartments and varying stiffness to study the interactions between OS cells and adipose-derived stem cells (ADSCs), found in the vicinity of *in vivo* OS masses. Saos2 cells and ADSCs were encapsulated in the central and outer donut-like compartments, respectively. Hydrogels composed of 75% GG and 25% SF presented a compressive modulus of ˜0.6 kPa and

promoted the formation of Saos2 spheroids and ADSC migration towards the core region, emphasizing the impact of mechanical properties on spheroid formation (**Figure 3** B).[88] Pavlou et al. [73] also developed 3D OS hydrogel-based models, with varying complexity, featuring a core collagen ACM (artificial cancer mass) region, with MG-63 or 143B cells, and a surrounding acellular ECM compartment, composed of collagen and laminin. The ACM and the acellular ECM were further enriched with cancellous bone granules (NuOSS®) and fibronectin, respectively, in the complex model. Both cell lines showed good viability and proliferation in the ACM, forming clusters that migrated towards the acellular ECM (**Figure 3** C). Compared with the basic model, the complex model demonstrated reduced spheroid migration, lower MMP-9 expression and increased doxorubicin resistance, particularly in the 143B cell line. [73]

dECM-based hydrogels have also been developed for *in vitro* OS cell culture, albeit the majority has been for bone regeneration studies, [156,157,158] while only a few *in vitro* dECM scaffolds have been produced to model and study OS[110,111]. For example, Zhao et al.[110] bioengineered an OS model by encapsulating MSCs in decellularized bone matrix. After their differentiation into osteoblasts, U2OS and HOS spheroids were seeded in the hydrogel. Compared to 2D or 3D scaffold-free spheroid cultures, this model exhibited an increased resistance to doxorubicin and cisplatin and was able to mimic the heterogeneity of native bone tumor tissue.[110] A more recent bone dECM model has been reported by Zhang et al. [111], which was able to sustain OS cell adhesion and proliferation. After demineralization and decellularization of mouse bones, the original porous structure, referred to as bone extracellular matrix (BEM), was preserved. MG-63 cells were injected into the medullary cavity of the bones and exhibited a heterogenous mesenchymal phenotype, similar to the observed *in vivo* . Moreover, cells either adhered to the remaining muscle residues and grew into aggregates or adhered to the bone matrix and proliferated.[111]

The high mineral content of the bone TME and the upregulation of bone mineralization pathways in OS suggest a possible role of the bone mineral phase in OS biology. Several 3D hydrogel-based models have, therefore, incorporated bioceramic compounds in the scaffolds, mainly HAp, to mimic the bone mineral phase. For example, Díaz et al.[78] demonstrated the importance of 3D scaffolds and bone mineral cues in mimicking the growth kinetics, chemoresistance and signaling patterns of *in vivo* OS tumors, by encapsulating MG-63 cells in gelatin scaffolds coated or not with HAp solutions. In contrast to 2D cultured cells, which proliferated faster, the 3D cultures mirrored the proliferation kinetics of *in vivo* tumors, exhibiting increased drug resistance and expression of the PI3K target. The presence of HAp nanoparticles further amplified these results and treatment with PI3K inhibitors inhibited tumor growth in 3D cultures.[78] Thus, using models with bone mineral cues can be useful to discover new potential drugs for OS, which may not be possible with 2D models or 3D models lacking such cues.

While scaffold-based models overcome the limitations of scaffold-free spheroid models, by introducing TME components, they do not effectively represent the cell-cell interactions observed within the tumor. This has, recently, prompted the embedment of 3D spheroids in biomimetic scaffolds, aiming to reproduce both cell-cell and cell-ECM interactions of *in vivo* tumors. As such, Monteiro et al.[159] demonstrated that modeling later and more invasive stages of OS could be achieved by encapsulating MG-63 spheroids in biomimetic GelMA and Matrigel® hydrogels. Compared with scaffold-free spheroids, the scaffold-based model presented higher cell viability, demonstrating the importance of including an ECM-mimetic matrix when modeling OS. Spheroids within the hydrogels maintained their morphology and invaded the surrounding matrix, whereas encapsulated single cells failed to establish the 3D *in vivo* macrostructure of OS, forming very few cellular agglomerates and showed higher sensitivity to chemotherapeutics. The authors concluded that the tumor cellular arrangement within scaffolds influences cell-cell adhesion, morphology and drug resistance, highlighting the need to consider these factors when modeling OS. [159] With these findings in mind, Monteiro et al. [160] investigated the effect of stroma cells in an OS spheroid-laden hydrogel. The 3D model incorporated MG-63 spheroids, osteoblasts and BM-MSCs encapsulated in methacryloyl platelet lysates (PLMA)-based hydrogels, to mimic tumor-stromal and cell-matrix interactions. PLMA, of human origin, was able to support human cell proliferation and the invasive phenotype of the spheroids. The tri-culture system exhibited increased cell viability, compared with monoculture PLMA scaffolds containing only the spheroids, and MSCs aligned towards the spheroids, eventually forming a network of cells directly interacting with the invasive

tumor cells.[160]

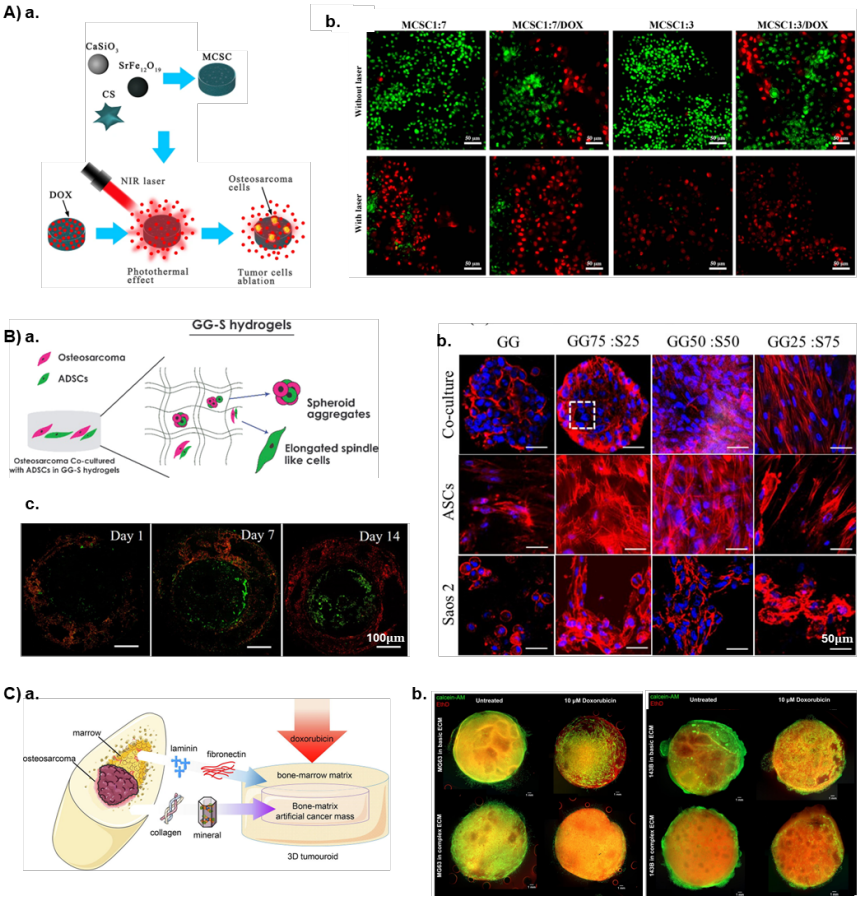

Figure 3. (A) (a) Schematics of the development of the magnetic chitosan films, with ferrite particles and silicate microspheres, by Yang et al. [153] (b) Live/dead imaging of MG-63 cells inside the scaffold after doxorubicin treatment, with and without NIR irradiation. Reproduced with permission. [153]Copyright 2018, Springer Nature. (B) (a) Schematics of the hydrogel-based model of OS developed by Kundu et al.[88]. (b) Confocal laser scanning micrographs of rhodamine-labelled phalloidin stained actin of the scaffolds, counterstained with DAPI, after co-culture of Saos2 cells and adipose stem cells (ADSCs) for 14 days. (c) Migration of ADSCs towards the Saos2 spheroids within the scaffold. ACSs and Saos2 cells are labelled with PKH26 Red Fluorescent Cell Linker and PKH67 Green Fluorescent Cell Linker. Reproduced with permission. [88] Copyright 2019 American Chemical Society (B) (a) Schematic diagram of the tumoroid models developed by Pavlou et al. [73]. (b) Fluorescent images of MG-63 and 143B basic and complex tumoroid models after 7 days of incubation. The Artificial Cancer Mass (ACM) margin is illustrated with a white-dotted line. (C) Live/dead imaging of the ACM compartment of the tumoroid models, treated or not with doxorubicin. Reproduced with permission. [73] Copyright 2019, Elsevier.

4.2.2 Electrospun fiber meshes

Electrospinning is a technique that produces nano- and micro-fibers by applying an electric field to a polymeric solution, which causes liquid droplets to become charged and experience electrostatic repulsing forces. When these forces overcome the liquid surface tension, a cone-shape jet is produced and extended along a straight line, being collected on a grounded collector as solid fibers.[161] By controlling the applied voltage,

the flow rate of the solution and the distance between the needle and the collector, fibers scaffolds with different diameters and porosities can be achieved. [162]

OS cells, specifically the MG-63 cell line, have been seeded on several types of electrospun fiber meshes. These range from collagen/gelatin,[163] alginate [62] and composite PVA/gelatin fibers [81] to more complex combinations, such as PVA/Silk Fibroin fibers with silver nanoparticles.[87] While these scaffolds were developed within the bone tissue engineering field, due to the osteoblastic-like behavior of this cell line, they showed that electrospun fibers can be used to mimic the ECM that supports the proliferation of OS cells. For example, Yeo et al.[62] combined cell-laden electrospun alginate fibers with PCL substrates, producing an interlayered scaffold in which MG-63 cells were able to proliferate. To achieve high cell viability and a homogeneous fiber mat, the applied electric field was optimized, as lower voltages caused less cell damage but were not successful in producing well-developed meshes. The reinforcement with PCL provided further mechanical support to the scaffold, supporting most of the stress applied to the scaffold during tensile testing.[62]

Nonetheless, the use of electrospinning to produce scaffold-based models of OS is still rather novel, with only a small number of models reported thus far. For example, to evaluate the OS response to different mechanical environments, Molina et al. [80]produced coaxial electrospun fibers, comprising a PCL core and a gelatin shell, with seeded MG-63 cells. The mechanical properties of the fibers were tuned, affecting fiber diameter and elastic moduli, by varying the PCL to gelatin ratio. The 3D environment induced lower expression (when compared with 2D monocultures) of the mechanoresponsive yes-associated protein (YAP), which has been linked to cancer proliferation and chemoresistance. The scaffold stiffness further affected YAP expression, with less stiffer scaffolds showing lower expression and increased YAP translocation to the nucleus, which contradicted initial hypotheses based on OS's mesenchymal origin and prior MSCs studies showing increased YAP translocation to the nucleus in stiffer environments. Additionally, the 3D environment led to the downregulation of the IGF-1R/mTOR pathway, linked to tumor growth and aggressiveness, reducing the efficacy of IGF-1R targeted agents combined with chemotherapy. The 3D architecture of the fiber meshes possibly induced a shift in the phenotype of MG-63 cells, no longer requiring the IGF1R/mTOR axis to proliferate, which emphasizes the need to incorporate mechanical cues in models developed for the study of OS pathogenesis.[80]

The complexity of this 3D OS model was later increased by Chim et al.[61], which introduced the OS immune niche, at least in part, by co-culturing MG-63 cells with TAMs in coaxial PCL/gelatin electrospun fibers. In scaffolds with moderate stiffness, the presence of TAMs induced an inflammatory response, characterized by higher levels of pro-inflammatory cytokines, such as IL-6, which contributed to an increased proliferation rate of OS cells and a decreased sensitivity to doxorubicin treatment. The inhibition of STAT3 (signal transducer and activator of transcription 3), which is a transcription factor activated by IL-6 that upregulates oncogenes, reduced the inflammation-mediated chemoresistance of OS cells by disrupting their crosstalk with TAMs, but did not increase doxorubicin efficacy. As such, signals from the immune niche should be considered during the development of new drugs for OS, as they can alter the chemosensitivity of cancer cells. [61]

4.2.3 3D bioprinted models

3D bioprinting allows the creation of 3D structures for cell culture, by depositing bioinks in a specific pattern, one layer at a time. Unlike 3D printing, where cells are merely seeded on top of the final constructs,[164,165] the incorporation of cells in 3D bioprinted models occurs before or during the printing process.[166,167] This allows a homogeneous cell distribution and the development of more relevant cell-cell and cell-ECM interactions, since cells are not just interacting with the substrate surfaces. Moreover, the spatial positioning of cells within the construct can be controlled, making it possible to create compartments with different cell types, which is of interest for the development of 3D biomimetic models of cancer with higher complexity.[24]

Bioinks are combinations of cells and/or biomaterials that serve as scaffolds for cell culture after bioprinting and crosslinking.[168] Depending on whether or not cells are dispersed in biomimetic materials, bioinks can be categorized as either scaffold-based or scaffold-free, respectively. Scaffold-free bioinks may contain spheroids,

cell pellets or tissue strands that produce their own ECM. However, bioinks are often hydrogel precursors that mimic the ECM and are crosslinked during or after bioprinting to retain the desired shape. [169] Due to their biomimicry properties, natural biomaterials are frequently used to produce bioinks for 3D bioprinted cancer models, but these usually have limited mechanical properties and lower stability, when compared with 3D printed scaffolds composed of synthetic materials. [24]For instance, Wang et al.[170] created a 3D printed OS model with similar stiffness and porosity of cortical bone, using poly-L-lactic acid (PLLA). The scaffolds were coated with dopamine for enhanced surface roughness and hydrophilicity and those with smaller pores supported the proliferation and adhesion of OS spheroids (MG-63, Saos-2 or HOS). The 3D environment stimulated a higher expression of ECM components (collagen, laminin and fibronectin), VEGF and TGF-β1, compared with 2D monolayers, indicating the potential of the 3D printed model to effectively mimic the bone TME. [170]

There are several methods for bioprinting 3D constructs, which can be classified based on how the bioink is deposited onto the surface. In extrusion-based bioprinting, the bioink is forced through a nozzle by pneumatic or mechanical actuation. This is the most popular bioprinting technique, since it enables the use of formulations with various viscosities, high cell densities and a wide variety of printable biomaterials. However, the structures are bioprinted at a slow speed and with low resolution, with cells being subjected to shear stress when they are pushed through the nozzle. [171]Inkjet-based has a fast-printing speed and high resolution, but only low viscosity biomaterials can be used. In this technique, the bioink is pushed through a nozzle in the form of droplets, by thermal or piezoelectric actuation. [172] On the other hand, in laser-based bioprinting, the bioink is deposited onto the target surface by using a focused laser beam that induces the release of bioink from a donor slide. This is a nozzle-free technique, thus avoiding the nozzle clogging drawback of the previous methods, and allows bioprinting with very fine detail, due to is high resolution. However, this method has a slower printing speed, high printing costs and presents the risk of UV-induced cellular damages. [173] Similarly, stereolithography bioprinting offers high spatial resolution and cell viability, but also carries the risk of cell toxicity, since the bioink is selectively crosslinked into a solid hydrogel, by photopolymerization. [174]

Similar to electrospun fiber meshes, 3D bioprinted scaffolds for OS cell culture have been mostly explored for bone tissue engineering applications. Nonetheless, these demonstrate the possibility of bioprinting OS cells with biomimetic materials and, therefore, developing 3D bioprinted OS models. For example, Neufurth et al. [97] studied the osteoblastic behavior of Saos-2 cells in a porous cylindrical 3D bioprinted model, using an alginate/gelatin bioink, which was easily crosslinked and had good cell adhesion properties. The bioprinted scaffold was overlaid with an agarose layer supplemented with polyphosphate (PolyP), which is synthesized by bone, resulting in a higher Young's modulus, increased structure stability, cell density and mineralization, as well as a similar proliferation rate of *in vivo* tumors, compared with non-overlaid scaffolds.[97] Following this study, the same team incorporated PolyP directly into the alginate/gelatin bioink and added culture media supplemented with nanoparticles of bioactive glass, a bone-mimicking bioceramic, which enhanced the mineralization of the 3D Saos-2-seeded bioprinted construct. [175] As such, alginate and gelatin can be used to bioprint OS cells and the inclusion of biologically active components, such as PolyP and bioactive glass, might also be important in 3D OS models to mimic the mineralized ECM.[175]

Still for bone regeneration purposes, Kim et al.[176] proposed a novel collagen-based bioink to bioprint MG-63 cells. To support high cell viability, genipin, a natural compound extracted from the gardenia fruit, was used as the crosslinking agent, since it allows a rapid crosslinking and is less cytotoxic than the typical collagen crosslinkers, such as EDC (1-ethyl-3-(3-dimethylaminopropyl) carbodiimide) or glutaraldehyde. While collagen bioprinted constructs are structurally not very stable, due to their low viscosity and poor mechanical properties, Kim and his team were able to produce a bioconstruct with enhanced stiffness by increasing the genipin concentration and crosslinking period.[176] Diamantides et al.[177] had previously reported that collagen bioinks with higher storage modulus before extrusion had better printability. Since the storage modulus of collagen solutions depends on the collagen and NaCl concentration and its temperature,[177] Kim et al. [176] also optimized the extrusion nozzle temperature to 10 ºC, which allowed the production of a collagen scaffold with stable pore geometry and interconnectivity. Compared to alginate bioprinted struc-

tures, this collagen-based scaffold presented higher cell viability, proliferation and metabolic activity, due to its higher biocompatibility, which makes this a promising platform for OS research. [176]Another way to increase the storage modulus of collagen bioinks and, therefore, their printability is to use a higher collagen concentration. However, the majority of collagen bioinks are produced from a low concentration solution, up to 10 mg/ml, since higher concentrations increase shear stress, thus decreasing cell viability.[178] Nonetheless, Pellegrin et al.[179] used a high-density collagen bioink (80 mg/mL), aiming to improve shape retention and the mechanical properties of the scaffold, and the bioprinted constructs supported the viability, proliferation and cluster formation of U2OS and cisplatin-resistant U2OS cells. Notably, the scaffold with resistant cells exhibited enhanced MMP-1 expression, matrix degradation and cell migration, attributed to a differential expression of collagen receptors on the surface of these cells. Additionally, the established 3D environment enhanced the expression of DNA repair enzymes, reducing the sensitivity to cisplatin. Compared with 2D cultures, this collagen 3D bioprinted model provided a better support for OS cells, allowing them to preserve their aggressive and invasive phenotype. [179]

Despite the promising potential of 3D bioprinting for the development of tumor models, only a few 3D bioprinted OS models have been reported. Recently, Lin et al. [180] used a GelMA/Methacrylated Hyaluronic Acid (HAMA) bioink, in which HOS or U2OS cells were encapsulated. The addition of HAMA resulted in an increased printability and the scaffold had a stiffness of 51 kPa, similar to the optimal matrix stiffness for OS-CSC enrichment, as reported by Jabbari et al. [115] While cell proliferation was observed, the 3D model exhibited downregulation of several genes related with cell cycle and metabolism, alongside overexpression of autophagy-related genes, in comparison with 2D cultures and scaffold-free spheroids. While autophagy removes damaged organelles and proteins, promoting cell survival, it may also lead to cell death, if activated in an excessive manner. Interestingly, the model showed higher sensitivity to autophagy inhibitors, rather than activators, revealing the pro-tumorigenic role of autophagy in OS. [180]In another recent study, Loi et al. [181]bioprinted OS cells within an ECM-mimetic bioink, based on gelatin and chitosan, optimized to achieve optimal printability and biocompatibility. The model allowed the study of OS cell migration, as cells were able to destroy the matrix, but, after one week, reduced cell viability was observed, probably due to stress from the bioprinting process. The fragmentation of the construct after 14 days indicated the need to increase the bioink resistance, which can be achieved by increasing the concentration of crosslinkers and changing the gelatin/chitosan ratio. [181]

Recent advances in biomaterial engineering and bioprinting have also encouraged the development of spheroid-laden and dECM-based bioinks to model cancer, especially for breast and prostate cancer.[107,182] So far, for OS models, there have not been reports of such bioinks, but ECM derived from MSCs has been incorporated by Negrini et al. [183] into a 3D printed polyurethane scaffold for modeling OS. Polyurethane, a synthetic material, was chosen to compose the ink due to its versatility, non-cytotoxicity and the possibility to control its mechanical properties, while the biomimetic environment was introduced by the ECM produced by MSCs that were seeded on the printed scaffolds. After the lysis of the MSC population, OS cells were seeded on the ECM-decorated scaffolds and interacted with the deposited ECM, which promoted their colonization. [183] As such, the use of dECM derived from OS cells seems to offer a more physiologically relevant platform for modeling OS.

4.3.4 Microfluidic models

Microfluidic devices are miniaturized systems that manipulate fluids and particles at the micron and submicron scale using micrometer-sized channels and chambers, offering a number of advantages over other *in vitro* platforms, including reduced sample sizes and precise control of fluid flow and perfusion. [184] These features have made them attractive for a variety of applications, such as gene and protein analysis, biosensing and high-throughput drug screening. [185] Recently, microfluidic technology has also been employed in cancer research to create *in vitro*microtumor models, since it allows the spatial and temporal manipulation of cells, gradients and ECM components of the TME.[186]

Regarding OS, a few microfluidic platforms have been developed to produce 3D *in vitro* models of the

disease, with or without the use of ECM-biomimetic materials. For example, Sarkar et al. [187] developed a 3D microfluidic spheroid model to study the effects of cellular stresses on the viability and VEGF secretion of MG-63 spheroids. The cells were distributed into multiple microchambers, through a microfluidic channel, and aggregated into spheroids of uniform size, exhibiting decreased viability and VEGF secretion in response to cellular stresses, such as nutrient deficiency and HIF inhibition. However, unlike 2D monolayers, exposure to higher levels of cellular stresses induced a higher secretion of VEGF by the spheroids, which suggests that the 3D architecture of the model supported a stronger resistance against higher cellular stresses, similar to what occurs *in vivo* , making this a relevant model of the OS-TME. [187] In another approach, Wei et al. [188] explored the use of microfluidic devices to create hollow doubled-layered microfibers for OS cell and HUVEC culture. The central microchannel of the device was filled with a hyaluronic acid solution, while the adjacent microchannels were perfused with cell-laden alginate solutions. By exposing the microchannels to a $CaCl_2$ bath, the alginate solutions were crosslinked, while the HA solution was dissolved, resulting in a hollow fiber construct, with an inner layer of HUVECs and an outer layer of MG-63 cells. Compared with single-layer constructs, the double-layered microfluidic model showed potential as a 3D *in vitro* OS model to be exploited in the future, as it sustained cell viability, allowed cells to spread and form cell-cell contacts, and exhibited an increased expression of osteogenic and vasculogenic genes. [188]

Microfluidic systems for 3D *in vitro* culture have also become commercially available. The OrganoPlate® Graft platforms (Mimetas, Inc.) are examples of such devices and are commonly used for tissue vascularization studies, in cancer and toxicology research, as they allow grafting the tissue under study onto a vascular bed.[189] The device features a central graft microchamber to place microtissues, such as spheroids, organoids and tissue explants, and microfluidic channels that can be filled with ECM-like hydrogels and/or culture media, with or without cells.[189] Using this platform, Avnet et al.[69] combined heterotypic spheroids of OS cells and MSCs with ECM-biomimetic materials to develop a 3D scaffold-based microfluidic model of OS. The spheroids were placed in the microchamber of the device, which was filled with a Matrigel/collagen hydrogel and passively perfused with acidic medium. The acidic microenvironment triggered an inflammatory response in MSCs, leading to the release of cytokines such as IL-6, which stimulated the migration of OS cells from the spheroids. These findings are in line with previous studies and demonstrate that IL-6 could be a target for inhibiting the migration of OS cells that survive acidosis *in vivo*.[69]

Table 2. Summary of 3D *in vitro* scaffold-based models of OS, including hydrogels, electrospun fibers, bioprinted structures and microfluidic devices.

Scaffold type	OS cell type	Co-culture cells	Therapeutic treatment	Therapeutic treatment	Findings	Ref
Hydrogels						
Matrigel®	HOS, 143B	–	–	sFRP2 knockdown in metastatic OS cells decreased their migrative and invasive potential.	sFRP2 knockdown in metastatic OS cells decreased their migrative and invasive potential.	[65]

Scaffold type	OS cell type	Co-culture cells	Therapeutic treatment	Therapeutic treatment	Findings	Ref
Matrigel® + Collagen	MOS, U2OS, KPD, ZK58, 143B and Saos-2	–	Trametinib, TKIs	OS cells with constitutive ERK phosphorylation were more sensitive to MEK inhibition.	OS cells with constitutive ERK phosphorylation were more sensitive to MEK inhibition.	[68]
Matrigel®	MG-63, U2OS	–	Doxorubicin	Overexpression of Syndecan-2 enhanced sensitivity to doxorubicin.	Overexpression of Syndecan-2 enhanced sensitivity to doxorubicin.	[66]
Matrigel® and collagen	MG-63	–	siRNA	VE-cadherin expression in OS cells was inhibited using siRNA technology, resulting in a reduction of angiogenic sprouting.	VE-cadherin expression in OS cells was inhibited using siRNA technology, resulting in a reduction of angiogenic sprouting.	[149]
Collagen	U2OS	–	Kinase inhibitor PI103	Cells exhibited a decreased proliferation rate and activation of the PI3K pathway in collagen hydrogels, compared with 2D monolayers. Stiffer scaffolds promoted a higher resistance of OS cells to PI103-induced inhibition of PI3K.	Cells exhibited a decreased proliferation rate and activation of the PI3K pathway in collagen hydrogels, compared with 2D monolayers. Stiffer scaffolds promoted a higher resistance of OS cells to PI103-induced inhibition of PI3K.	[72]

Scaffold type	OS cell type	Co-culture cells	Therapeutic treatment	Therapeutic treatment	Findings	Ref
Collagen	–	–	–	Cells had a rounder cell shape and reduced secretion of MMP-2 when cultured in 3D collagen hydrogels, compared with 2D collagen layers.	Cells had a rounder cell shape and reduced secretion of MMP-2 when cultured in 3D collagen hydrogels, compared with 2D collagen layers.	[150]
Collagen, Matrigel®, agarose and alginate	MG-63	–	–	Different hydrogels were produced, with varying degrees of elasticity and adhesive properties. MG-63 cells exhibited higher viability and proliferation in scaffolds with higher mechanical elasticity.	Different hydrogels were produced, with varying degrees of elasticity and adhesive properties. MG-63 cells exhibited higher viability and proliferation in scaffolds with higher mechanical elasticity.	[151]
Silk fibroin	143B	–	–	The expression of angiogenic markers (HIF-1α and VEGF) by OS cells was increased in the 3D hydrogel, compared with 2D monolayers.	The expression of angiogenic markers (HIF-1α and VEGF) by OS cells was increased in the 3D hydrogel, compared with 2D monolayers.	[89]

Scaffold type	OS cell type	Co-culture cells	Therapeutic treatment	Therapeutic treatment	Findings	Ref
Silk fibroin	U2OS, Saos-2	–	Doxorubicin, Cisplatin	OS cells showed a G1 cell cycle arrest and reduced proliferation in the 3D model, along with higher resistance to doxorubicin, compared with 2D monolayers. Treatment with cisplatin showed no significant differences between the two culture methods.	OS cells showed a G1 cell cycle arrest and reduced proliferation in the 3D model, along with higher resistance to doxorubicin, compared with 2D monolayers. Treatment with cisplatin showed no significant differences between the two culture methods.	[90]
PEGDA	U2OS	–	–	The CSC subpopulation of OS cells was mainly enriched in hydrogels with stiffness of 55 kPa.	The CSC subpopulation of OS cells was mainly enriched in hydrogels with stiffness of 55 kPa.	[115]
Chitosan	MG-63	–	$CaSiO_3$ microspheres loaded with doxorubicin and ferrite particles	Exposure to near infrared radiation induced a more localized release of doxorubicin, through the ferrite particles, resulting in an increased cytotoxicity to OS cells.	Exposure to near infrared radiation induced a more localized release of doxorubicin, through the ferrite particles, resulting in an increased cytotoxicity to OS cells.	[153]

Scaffold type	OS cell type	Co-culture cells	Therapeutic treatment	Therapeutic treatment	Findings	Ref
Collagen + HAp particles	MG-63	–	Plasma-activated solution	The 3D environment had a protective role against the oxidative stress generated by CAP, by scavenging ROS and upregulating the expression of CSC-related genes.	The 3D environment had a protective role against the oxidative stress generated by CAP, by scavenging ROS and upregulating the expression of CSC-related genes.	[74]
Alginate + gelatin	MG-63	–	–	Cells proliferated within the gelatin core, showing an increased expression of osteogenic markers, compared with the 2D *in vitro* model. The alginate-shell of the capsule enhanced its stability.	Cells proliferated within the gelatin core, showing an increased expression of osteogenic markers, compared with the 2D *in vitro* model. The alginate-shell of the capsule enhanced its stability.	[96]
Gellan Gum + Silk Fibroin	Saos-2	ADSCs[a)]	–	Saos-2 cells formed spheroids and ADSCs migrated towards them in hydrogels with a specific stiffness of ˜0.6 kPa.	Saos-2 cells formed spheroids and ADSCs migrated towards them in hydrogels with a specific stiffness of ˜0.6 kPa.	[88]

Scaffold type	OS cell type	Co-culture cells	Therapeutic treatment	Therapeutic treatment	Findings	Ref
Collagen + laminin + fibronectin, bone granules	MG-63, 143B	–	–	The supplementation with bone cancellous granules induced a decreased invasion of OS cells, lower expression of MMP-9 and increased resistance to doxorubicin.	The supplementation with bone cancellous granules induced a decreased invasion of OS cells, lower expression of MMP-9 and increased resistance to doxorubicin.	[73]
Gelatin + HAp nanoparticles	MG-63	–	Doxorubicin	The presence of HAp particles promoted a higher resistance of OS cells to doxorubicin, possibly related with the increased activation of the IGF-1R pathway.	The presence of HAp particles promoted a higher resistance of OS cells to doxorubicin, possibly related with the increased activation of the IGF-1R pathway.	[78]
GelMA and Matrigel	MG-63 (single-cells or spheroids)	–	Lorlatinib	Encapsulated spheroids invaded the surrounding matrix and showed a higher resistance to lorlatinib, compared with cell-laden hydrogels.	Encapsulated spheroids invaded the surrounding matrix and showed a higher resistance to lorlatinib, compared with cell-laden hydrogels.	[159]

Scaffold type	OS cell type	Co-culture cells	Therapeutic treatment	Therapeutic treatment	Findings	Ref
PLMA[b)]	MG-63 (spheroids)	hOB[c)] and hBM-MSC	Doxorubicin	The triculture system presented higher tumor cell viability, invasive ability and drug resistance, compared with hydrogels in which only spheroids were encapsulated.	The triculture system presented higher tumor cell viability, invasive ability and drug resistance, compared with hydrogels in which only spheroids were encapsulated.	[160]
Decellularized bone matrix	U2OS, HOS (spheroids)	MSCs (differentiated into OBs)	Doxorubicin, cisplatin	Spheroids encapsulated in dECM-based scaffolds exhibited higher drug resistance, compared to 2D and 3D scaffold-free spheroids.	Spheroids encapsulated in dECM-based scaffolds exhibited higher drug resistance, compared to 2D and 3D scaffold-free spheroids.	[110]
Decellularized bone mouse	MG-63	–	–	MG-63 cells showed a heterogeneous phenotype and proliferated within the bone matrix. Cellular aggregates were also observed.	MG-63 cells showed a heterogeneous phenotype and proliferated within the bone matrix. Cellular aggregates were also observed.	[111]
Electrospun fibers	*Electrospun fibers*					

Scaffold type	OS cell type	Co-culture cells	Therapeutic treatment	Therapeutic treatment	Findings	Ref
Alginate + PCL	MG-63	–	–	Cells proliferated within the alginate fibrous mesh, while the use of PCL enhanced the mechanical properties of the structure.	Cells proliferated within the alginate fibrous mesh, while the use of PCL enhanced the mechanical properties of the structure.	[62]
PVA + gelatin	MG-63	–	–	The scaffolds supported cell proliferation and adhesion due to their hydrophilic properties.	The scaffolds supported cell proliferation and adhesion due to their hydrophilic properties.	[81]
PVA + silk fibroin + Ag nanoparticles	MG-63	–	–	Composite fiber constructs showed a higher cell viability, ECM matrix production and tensile strength, compared with pure PVA fibers.	Composite fiber constructs showed a higher cell viability, ECM matrix production and tensile strength, compared with pure PVA fibers.	[87]

Scaffold type	OS cell type	Co-culture cells	Therapeutic treatment	Therapeutic treatment	Findings	Ref
PCL (core) + gelatin (shell)	MG-63	–	–	Cells penetrated the fiber meshes and showed a reduced expression of YAP, especially in stiffer scaffolds, compared with 2D models.	Cells penetrated the fiber meshes and showed a reduced expression of YAP, especially in stiffer scaffolds, compared with 2D models.	[80]
PCL (core) + gelatin (shell)	MG-63	TAMs	Doxorubicin	The presence of TAMs induced an inflamma-tory response and secretion of IL-6, which promoted a higher resistance of OS cells to doxorubicin.	The presence of TAMs induced an inflamma-tory response and secretion of IL-6, which promoted a higher resistance of OS cells to doxorubicin.	[61]
3D bioprinted scaffolds	*3D bioprinted scaffolds*					
Alginate + gelatin	Saos-2	–	–	The scaffold was coated with agarose and PolyP, which increased its stability and cell density. Cells showed a similar proliferation rate of *in vivo* tumors.	The scaffold was coated with agarose and PolyP, which increased its stability and cell density. Cells showed a similar proliferation rate of *in vivo* tumors.	[97]

Scaffold type	OS cell type	Co-culture cells	Therapeutic treatment	Therapeutic treatment	Findings	Ref
Alginate + gelatin + PolyP[d)]	Saos-2	–	–	When exposed to biologically active components, such as PolyP and bioactive glass, the scaffolds promoted a higher mineralization of OS cells.	When exposed to biologically active components, such as PolyP and bioactive glass, the scaffolds promoted a higher mineralization of OS cells.	[175]
Collagen	MG-63	–	–	The collagen scaffold was crosslinked with genipin, showing good structural stability and promoting high cell viability, proliferation and metabolic activity of OS cells.	The collagen scaffold was crosslinked with genipin, showing good structural stability and promoting high cell viability, proliferation and metabolic activity of OS cells.	[176]
Collagen	U2OS	–	Cisplatin	The bioprinted structure had favorable mechanical properties, sustained the viability and proliferation of OS cells and increased their resistance to cisplatin.	The bioprinted structure had favorable mechanical properties, sustained the viability and proliferation of OS cells and increased their resistance to cisplatin.	[179]

Scaffold type	OS cell type	Co-culture cells	Therapeutic treatment	Therapeutic treatment	Findings	Ref
GelMA + HAMA[e)]	HOS, U2OS	–	Everolimus, Chloroquine	The addition of HAMA increased the bioinks' printability, and the model showed an increased resistance of OS cells to autophagy inhibitors	The addition of HAMA increased the bioinks' printability, and the model showed an increased resistance of OS cells to autophagy inhibitors	[180]
Gelatin + chitosan	UMR-106	–	–	The bioink presented good printing resolution and supported the migration of OS cells.	The bioink presented good printing resolution and supported the migration of OS cells.	[181]
Polyurethane	Saos-2	MSCs	–	OS cells interacted with the ECM secreted by MSCs, previously seeded on the scaffolds, which promoted their migration.	OS cells interacted with the ECM secreted by MSCs, previously seeded on the scaffolds, which promoted their migration.	[183]
Microfluidic platforms	*Microfluidic platforms*					

Scaffold type	OS cell type	Co-culture cells	Therapeutic treatment	Therapeutic treatment	Findings	Ref
–	MG-63	–	–	Cells aggregated into spheroids in the microwells of the platform, showing decreased viability and VEGF secretion in response to nutrient deficiency and HIF inhibition.	Cells aggregated into spheroids in the microwells of the platform, showing decreased viability and VEGF secretion in response to nutrient deficiency and HIF inhibition.	[187]
Matrigel® + collagen	OS	MSCs	–	When exposed to acidic conditions, MSCs secreted IL-6 which induced the migration of OS cells from OS/MSC spheroids.	When exposed to acidic conditions, MSCs secreted IL-6 which induced the migration of OS cells from OS/MSC spheroids.	[69]
Alginate	MG-63	HUVECs	–	OS cells and HUVECs encapsulated in double-layered fibers presented a higher expression of osteogenic and vasculogenic genes, compared with single-layered fibers.	OS cells and HUVECs encapsulated in double-layered fibers presented a higher expression of osteogenic and vasculogenic genes, compared with single-layered fibers.	[188]

[a)] ADSCs: Adipose-derived stem cells;[b)] PLMA: Methacryloyl platelet lysates;[c)] hOB: human osteoblasts; [d)] PolyP: polyphosphate; [e)] HAMA: methacrylated hyaluronic acid.

5. Future Perspectives

Significant progress has been achieved in the development of 3D *in vitro* models of OS, progressing from simple tumor spheroids, generated with scaffold-free techniques, [54,128,135] to more complex scaffold-based models, incorporating biomaterials that recapitulate the TME. [68,89,150] While spheroids are recognized as superior models for replicating the 3D structure of the tumor, their ability to accurately represent the TME is compromised by the absence of a biomimetic scaffold. Consequently, the ongoing efforts to integrate tumor spheroids with scaffolds are considered a promising avenue for advancing *in vitro* OS modeling.

Enhancing the reliability of 3D *in vitro* models also requires the representation of the characteristic immune system and vascularization of OS. [190] While some spheroid- and hydrogel-based models have attempted to simulate these environments,[61, 140] there is still room for improvement. For instance, exploring 3D patterning of cells, through techniques such as 3D bioprinting and microfluidic technology, can enable more precise representations of the architectural complexity observed in *in vivo* OS tumors.[191] In this context, while not directly related to *in vitro* OS modeling, there have been reports of successful 3D bioprinting involving pre-formed breast cancer spheroids, both in monoculture and co-cultured with endothelial cells.[182] The spheroids were able to maintain their 3D structure, polarity and function, suggesting that the physical stress of bioprinting did not compromise their integrity.[182] Moreover, microfluidic technology has also allowed the creation of tumor models with perfusion. Aung et al.[192] used this strategy to develop a vascularized breast tumor-on-a chip: single HUVECs and breast cancer spheroids were encapsulated in GelMA hydrogels and cultured within a microfluidic platform. By controlling the device's flow rate, a chemoattractant gradient was created, promoting the formation of an endothelial-like barrier, while the spheroids remained at the center of the hydrogel. Exposure to high doses of doxorubicin resulted in reduction of spheroid size and loss of the endothelial barrier, showcasing the drug's non-specificity. [192] Both these strategies could be easily translated to OS research.

As emphasized in this review, the development of 3D *in vitro* OS models commonly involves the use of commercial OS cell lines, including the U2OS, MG-63, Saos-2 and HOS cell lines. The selection of which cell line to use usually depends on the specific objective of the model, whether it aims to replicate the migratory types of OS tumors, clonogenic characteristics, metastatic potential, aggressiveness and so forth. [53] However, it is noteworthy that these cancer cell lines were established in the 1970-80s and have likely adapted to long term *in vitro* culture, losing the cellular heterogeneity of the original tumor, [129] which emphasizes the need for patient-derived biological samples.

Tumor organoids, derived from primary tumor tissues, are presented as advanced 3D *in vitro* models that faithfully retain the heterogeneity, histologic architecture and cell-ECM interactions of the original tumor, being valuable tools for the development of personalized treatments. [190,193] They are obtained from fresh biopsies, which are mechanically or enzymatically digested and cultured in an ECM-like structure – typically Matrigel® or collagen layers – with specialized media conducive to organoid-like growth and maintenance. [190] While tumor spheroids – which are typically generated from commercial cancer cell lines in a scaffold-free manner – are able to mirror metabolic and proliferation gradients of *in vivo* tumors, they exhibit lower complexity in representing the tumor organization compared to organoids.[194] As such, with their long-term culture potential and cryopreservability, organoids are more histologically relevant tumor models, recapitulating both the structural and functional complexity of the original tumor tissue. [195]

Within cancer research, organoids have been predominantly employed to model epithelial-type cancers, given the availability of patient-derived material from these cancer types. [196,197,198] In contrast, there has been limited progress in the development of organoids specifically related to sarcomas, including OS. He et al.[199] explored the generation of organoids from primary and lung metastatic OS tissues, using two

methods: EnBloc culture and single cell suspension culture. Patient-derived specimens were cultured in collagen layers within a transwell insert (EnBloc) or as single cell suspensions in Matrigel®. Organoids from lung metastatic OS tissues, formed within 7 days, had similar morphology and histopathology to their parent tumor tissues, displaying negative TP53 expression, positive SOX9 expression and featuring tumor-infiltrating lymphocytes. Additionally, they were cryopreserved without loss in viability, suggesting the possibility of creating organoid biobanks. As such, this organoid culture system for OS holds promise for antitumor drug screening and for evaluating immunotherapy.[199] In a more recent study, Johansson et al.[200] was also able to generate organoids from cryopreserved OS cancer cells, previously obtained from patients through surgery or endoscopic biopsies. They used a basement membrane extracted (BME)-gel and cultured the organoids in media supplemented with various growth factors, revealing an augmented VEGF secretion with serial passaging. [200]

Despite these preliminary studies, the development of OS organoids still remains relatively unexplored, primarily due to the limited access to patient-derived samples, given the rarity of this cancer type.[201] Moreover, although the diagnosis requires a tumor biopsy, challenges persist in optimizing the composition of the culture media for organoid growth: in contrast to epithelial-based tumors, sarcomas, like OS, typically exhibit a heterogeneous cell population with more diverse intra-tumoral morphological and genotypic features, which makes the maintenance of each cell type more challenging. [194]

6. Conclusions

In OS research, bioengineered 3D *in vitro* models have emerged as valuable platforms, bridging the gap between 2D *in vitro*monocultures and animal models. They offer a more representative depiction of the TME, incorporating relevant cell-cell interactions within a 3D macrostructure, and potentially reduce the need for animal testing. Different techniques have been employed to develop these models, ranging from simple scaffold-free spheroid culture systems and hydrogel-based scaffolds, to more complex electrospun fiber meshes, integrative microfluidic platforms and complex 3D bioprinted scaffolds. While 3D *in vitro* models have enhanced our understanding of OS, namely regarding the efficacy of MAP chemotherapy, the invasive behavior of OS cells, the activation of cancer-related pathways and the influence of matrix stiffness and the 3D spatial configuration on chemoresistance, there still remains an urgent need for more robust preclinical models with a higher level of OS biomimicry. Future research should focus on integrating spheroids with scaffold-based techniques, introducing additional stromal cell types to simulate the tumor vascularization and immune environment of OS, and incorporating perfusion into the model – particularly important for evaluating novel treatments. Despite these challenges, the extensive knowledge acquired to date clearly demonstrates the importance of using 3D *in vitro* models in preclinical OS research.

Acknowledgements

The authors acknowledge funding from FCT—Portuguese Foundation for Science and Technology (FCT/MCTES), with dedicated funding from the projects eOnco (2022.07252.PTDC) and InSilico4OCReg (PTDC/EME-SIS/0838/2021), and also through institutional funds to iBB (UIDB/04565/2020 and UIDP/04565/2020) and Associate Laboratory i4HB (LA/P/0140/2020). This project also received financial support from “la Caixa” Foundation (ID 100010434) LCF/BQ/PI22/11910025.

References

[1] I. Corre, F. Verrecchia, V. Crenn, F. Redini, V. Trichet, *Cells* **2020** *9* , 976.

[2] Sarcoma: What it is, Symptoms & Treatment, https://my.clevelandclinic.org/health/diseases/17934-sarcoma, accessed: August, 2023.

[3] A. Misaghi, A. Goldin, M. Awad, A. A. Kulidjian, *SICOT-J***2018** , *4* , 12.

[4] R. A. Durfee, M. Mohammed, H. H. Luu, *Rheumatol.Ther* . **2016** , *3* , 221.

[5] A. Abarrategi, J. Tornin, M. C. Lucia, A. Hamilton, M. C. Enrique, J. P. Rodrigo, M. V. González, N. Baldini, G. C. Javier, R. Rodriguez, *Stem Cells Int* . **2016** , *2016* , 3631764.

[6] Y. Ağirdil, *EFORT Open Reviews* **2020** , *5* , 498.

[7] G. A. Odri, J. Tchicaya-Bouanga, D. J. U. Yoon, D. Modrowski, D.*Cancers* **2022** , *14* , 360.

[8] Z. S. Kundu, *Indian J. Orthop.* **2014** , *48* , 238.

[9] S. A. Savage, L. Mirabello, *Sarcoma* **2011** ,*2011* , 548151.

[10] M. Hameed, D. Mandelker, *Adv. Anat. Pathol* .**2018** , *25* , 217.

[11] Survival rates for osteosarcoma, https://www.cancer.org/cancer/types/osteosarcoma/detection-diagnosis-staging/survival-rates.html, accessed: August, **2023** .

[12] T. Ozaki, A. Nakagawara, *Cancers* **2011** ,*3* , 994.

[13] C. Giacinti, A. Giordano, *Oncogene* **2006** ,*25* , 5220.

[14] J. Rodrigues, B. Sarmento, C. L. Pereira, *In vitro models* **2022** , *1* , 5.

[15] N. Rainusso, T.-K. Man, C. C. Lau, J. Hicks, J. J. Shen, A. Yu, L. L. Wang, J. M. Rosen, *Cancer Biol. Ther.* **2011** ,*12* , 278.

[16] S. R. Martins-Neves, A. O Lopes, A. Carmo, A. A. Paiva, P. C. Simões, A. J. Abrunhosa, C. M. Gomes, *BMC Cancer* **2012** ,*12* , 139. [17] H.-M. Zhou, J.-G. Zhang, X. Zhang, W. Li, *Signal Transduct. Target. Ther* . **2021** , *6* , 62.

[18] X. Yu, T. G. Pestell, M. P. Lisanti, R. G. Pestell, R. G.*Int. J. Biochem . Cell Biol.* **2012** , *44* , 2144.

[19] C. Jubelin, J. Muñoz-Garcia, L. Griscom, D. Cochonneau, E. Ollivier, M. F. Heymann, F. M. Vallette, L. Oliver, D. Heymann,*Cell Biosci.* **2022** , *12* , 155. [20] M. Kapałczyńska, T. Kolenda, W. Przybyła, M. Zajaczkowska, A. Teresiak, V. Filas, M. Ibbs, R. Bliźniak, L. Łuczewski,, K. Lamperska,*Arch. Med. Sci.* **2018** , *14* , 910.

[21] X. Lin, S. Patil, Y.-G. Gao, A. Qian, *Front. Pharmacol.***2020** , *11* , 5.

[22] A. M. Mohamed, *Malays J Med Sci* . **2008** ,*15* , 4.

[23] M. S. Carvalho, J. M. S. Cabral, C. L. da Silva, D. Vashishth,*Polymers (Basel, Switz.)* **2021** , *13* , 1095.

[24] T. Fischetti, G. D. Pompo, N. Baldini, S. Avnet, G. Graziani,*Cancers* **2021** , *13* , 4065.

[25] M. B. Schaffler, O. D. Kennedy, *Curr. Osteoporos. Rep* .**2012** , *10* , 118.

[26] L. Zhu, Y. Tang, X.-Y. Li, E. T. Keller, J. Yang, J.-S. Cho, T. Y. Feinberg, S. J. Weiss, *Sci. Transl. Med* . **2020** , *12* , eaaw6143.

[27] B. F. Boyce, L. Xing, *Arch. Biochem. Biophys.***2008** , *473* , 139.

[28] J.-M. Kim, C. Lin, Z. Stavre, M. B. Greenblatt, J.-H. Shim,*Cells* **2020** , *9* , 2073.

[29] A. Alfranca, L. Martinez-Cruzado, J. Tornin, A. Abarrategi, T. Amaral, E. de Alava, P. Menendez, J. Garcia-Castro, R. Rodriguez,*Cell. Mol. Life Sci* . **2015** , *72* , 3097.

[30] E. Rothzerg, J. Xu, D. Wood, *J. Mol. Pathol.***2023** , *4* , 99.

[31] L. Zhu, M. M. McManus, D. P. M. Hughes, *Front. Oncol.***2013** , *3* , 230.

[32] W. Zeng, R. Wan, Y. Zheng, S. R. Singh, Y. Wei, *Cancer Lett.* **2011** , *313* , 129.

[33] Y. Li, L. Zhao, X.-F. Li, *Technol. Cancer Res. Treat.***2021** , *20* , 129.

[34] B. L. Krock, N. Skuli, M. C. Simon, *Genes Cancer***2011** , *2* , 1117.

[35] J. Zeng, Y. Peng, D. Wang, K. Ayesha, S. Chen, *Front. Cell Dev. Biology* **2023** , *11,* 1123065.

[36] X.-S Cai, Y.-W. Jia, J. Mei, R.-Y. Tang, *Chin. Med. J.***2004** , *117* , 94.

[37] F. Cersosimo, S. Lonardi, G. Bernardini, B. Telfer, G. E. Mandelli, A. Santucci, W. Vermi, E. Giurisato. *Int. J. Mol. Sci* .**2020** , *21* , 5207.

[38] T. Zhu, J. Han, L. Yang, Z. Cai, W. Sun, Y. Hua, J. Xu,*Front. Immunol.* **2022** , *13* , 907550.

[39] Z. Gao, G.-S. Zhao, Y. Lv, D. Peng, X. Tang, H. Song, Q.-N. Guo, *Oncol. Rep* . **2019** , *41* , 235.

[40] Z. Zhang, Z. Zhu, J. Fu, X. Liu, Z. Mi, H. Tao, H. Fan,*Int. Immunopharmacol.* **2023** , *115* , 109684.

[41] A. Mazumdar, J. Urdinez, A. Boro, J. Migliavacca, M. J. E. Arlt, R. Muff, B. Fuchs, J. G. Snedeker, A. Gvozdenovic, *Int. J. Mol. Sci* . **2020** , *21* , 5451.

[42] G. A. Odri, J. Tchicaya-Bouanga, D. J. Y. Yoon, D. Modrowski,*Cancers* **2022** , *14* , 360.

[43] A. D. Luca, L. Raimondi, F. Salamanna, V. Carina, V. Costa, D. Bellavia, R. Alessandro, M. Fini, G. Giavaresi, *J. Exp. Clin. Cancer. Res.* **2018** , *37* , 2.

[44] H. Sajjad, S. Imtiaz, T. Noor, Y. H. Siddiqui, A. Sajjad, M. Zia, *Anim. Models Exp. Med.* **2021** , *4* , 87.

[45] M. Cortini, N. Baldini, S. Avnet, *Front. Physiol.***2019** , *10,* 814.

[46] L. Tan, Y. Wang, X. Hu, G. Du, X. Tang, L. Min,*Biomolecules* **2023** , *13* , 1362. [47] B. M. Baker, C. S. Chen, *J. Cell Sci.* **2012** ,*125* , 3015.

[48] F. Pu, H. Guo, D. Shi, F. Chen, Y. Peng, X. Huang, J. Liu, Z. Zhang, Z. Shao, *Genes Dis.* **2023** , *11* , 664. [49] G. J. Yoshida, J. Hematol. Oncol. **2020** , *13* , 4.

[50] N. G. Frangogiannis, *J. Cardiovasc. Aging* **2022** ,*2* , 22.

[51] C. F. Monteiro, C. A. Custódio, J. F. Mano, *Adv. Therap.***2019** , *2* , 1800108. [52] B. Blanco-Fernandez, V. M. Gaspar, E. Engel, J. F. Mano,*Adv. Sci.* **2021** , *8* , 2003129.

[53] S. U. Lauvrak, E. Munthe, S. H. Kresse, E. W. Stratford, H. M. Namløs, L. A. Meza-Zepeda, O. Myklebost, *Br. J. Cancer***2013** , *109* , 2228.

[54] S. K. Marshall, B. Saelim, M. Taweesap, V. Pachana, Y. Panrak, N. Makchuchit, P. Jaroenpakdee, *Nanomaterials* **2022** ,*12* , 3517.

[55] M. T. Santini, G. Rainaldi, R. Romano, A. Ferrante, S. Clemente, A. Motta, P. L. Indovina, *FEBS Lett.* **2004** ,*557* , 148.

[56] P. Indovina, G. Rainaldi, M. T. Santini, *Anticancer res.***2008** , *28* , 1013.

[57] M.-H. Hsieh, J.-S. Yang, R.-C. Lin, Y.-H. Hsieh, S.-F. Yang, H.-R. Chang, K.-H. Lu, *Molecules* **2020** , *25* , 326.

[58] L.-T. Yeh, C.-W. Lin, K.-H. Lu, Y.-H. Hsieh, C.-B. Yeh, S.-F. Yang, J.-S. Yang, *Int. J. Mol. Sci* . **2022** , *23* , 484.

[59] C. Liu, P. Zhao, Y. Yang, X. Xu, L. Wang, B. Li, *Mol. Med. Rep.* **2016** , *13* , 4729.

[60] T. Chow, I. Wutami, E. Lucarelli, P. F. Choong, S. Duchi, C. D. Bella, *Tissue Eng., Part B* **2021** , 27, 514.

[61] L. K. Chim, I. L. Williams, C. J. Bashor, A. G. Mikos,*Biomaterials* **2023** , *296* , 122076.

[62] M. Yeo, G. Kim, *Chem. Eng. J.* **2015** , *275* , 27.

[63] E. R. Molina, L. K. Chim, M. C. Salazar, G. L. Koons, B. A. Menegaz, A. Ruiz-Velasco, S.-E. Lamhamedi-Cherradi, A. M. Vetter, T. Satish, B. Cuglievan, M. M. Smoak, D. W. Scott, J. A. Ludwig, A. G. Mikos, *ACS Biomater. Sci. Eng.* **2020** , *6* , 539.

[64] Cultrex 3-D culture matrix reduced growth factor basement membrane extract. https://shorturl.at/yAVYZ, accessed: August,**2023**[65] P. Techavichit, Y. Gao, L. Kurenbekova, R. Shuck, L. A. Donehower, J. T. Yustein, *BMC Cancer* **2016** , *16* , 11.

[66] A. Orosco, O. Fromigue, C. Bazille, N. Entz-Werle, P. Levillain, P. J. Marie, D. Modrowski, *Cancer Res.* **2007** ,*67* , 3708.

[67] M. Gorska, P. B. Krzywiec, A. Kuban-Jankowska, M. Zmijewski, M. Wozniak, J. Wierzbicka, A. Piotrowska, K. Siwicka, *Anticancer Res.* **2016** , *36* , 221.

[68] Z. Baranski, T. H. Booij, M. L. Kuijjer, Y. D. Jong, A.-M. Cleton-Jansen, L. S. Price, B. V. D. Water, J. V. M. G. Bov ée, P. C. W. Hogendoorn, E. H. J. Danen, *Genes Cancer* **2015** , *6* , 503.

[69] S. Avnet, S. Lemma, M. Cortini, G. D. Pompo, F. Perut, M. V. Lipreri, L. Roncuzzi, M. Columbaro, C. Errani, A. Longhi, N. Zini, D. Heymann, M. Dominici, G. Grisendi, G. Golinelli, L. Consolino, D. L. Longo, C. Nanni, A. Righi, N. Baldini, *Cancers* **2021** ,*13* , 5855.

[70] I. N. Amirrah, Y. Lokanathan, I. Zulkiflee, M. F. M. R. Wee, A. Motta, M. B. Fauzi, *Biomedicines* **2022** , *10* , 2307. [71] K. M. Charoen, B. Fallica, Y. L. Colson, M. H. Zaman, M. W. Grinstaff, *Biomaterials* **2014** , *35* , 2264.

[72] B. Fallica, J. S. Maffei, S. Villa, G. Makin, M. Zaman,*PLoS ONE* **2012** , *7* , e48024.

[73] M. Pavlou, M. Shah, P. Gikas, T. Briggs, S. Roberts, U. Cheema,*Acta Biomater.* **2019** , *96* , 247.

[74] J. Tornín, A. Villasante, X. Solé-Martí, M.-P. Ginebra, C. Canal, *Free Radical Biol. Med.* **2021** , *164* , 107.

[75] A. B. Bello, D. Kim, D. Kim, H. Park, S.-H. Lee, *Tissue Eng., Part B* **2020** , *26* , 164.

[76] T. U. Rashid, S. Sharmeen, S. Biswas, T. Ahmed, A. K. Mallik, M. Shahruzzaman, M. N. Sakib, P. Haque, M. M. Rahman, *Polymers and Polymeric Composites: A Reference Series* , Springer International Publishing, **2019** ; 1601.

[77] A. Cerchiari, J. C. Garbe, M. E. Todhunter, N. Y. Jee, J. R. Pinney, M. A. LaBarge, T. A. Desai, Z. J. Gartner, *Tissue Eng., Part C* **2015** , *21* , 541.

[78] E. C. G. Díaz, A. G. Lee, L. C. Sayles, C. Feria, E. A. Sweet-Cordero, F. Yang, *Adv. Healthcare Mater.* **2022** ,*11* , 2200768.

[79] T. Jiang, J. Zhao, S. Yu, Z. Mao, C. Gao, Y. Zhu, C. Mao, L. Zheng, *Biomaterials* **2019** , *188* , 130.

[80] E. R. Molina, L. K. Chim, M. C. Salazar, S. M. Mehta, B. A. Menegaz, S.-E. Lamhamedi-Cherradi, T. Satish, S. Mohiuddin, D. McCall, A. M. Zaske, B. Cuglievan, A. J. Lazar, D. W. Scott, J. K. Grande-Allen, J. A. Ludwig, A. G. Mikos, *Acta Biomater.* **2019** ,*100* , 38.

[81] N. T. B. Linh B.-T. Lee, *J. Biomater. Appl.***2012** , *27* , 255.

[82] K. Yue, G. Trujillo-de Santiago, M. M. Alvarez, A. Tamayol, N. Annabi, A. Khademhosseini, A. *Biomaterials* **2015** , *73* , 254.

[83] C. Lujerdean, G.-M. Baci, A.-A Cucu, D. S. Dezmirean,*Insects* **2022** , *13* , 286. [84] G. Li, S. Sun, *Molecules* **2022** , *27* , 2757.

[85] H. Wu, K. Lin, C. Zhao, X. Wang, *Front. Bioeng. Biotechnol.* **2022** , *10,* 1054379.

[86] L. Lin, R. Hao, W. Xiong, J. Zhong, *J. Biosci. Bioeng.***2015** , *119* , 591.

[87] M. L. M. Suaza, J. C. L. Rivera, M. C. R. Padilla, M. E. M. Acevedo, C. P. O. Orozco, D. G. Z. Triviño, *Polymers***2023** , *15* , 1838.

[88] B. Kundu, A. R. Bastos, V. Brancato, M. T. Cerqueira, J. M. Oliveira, V. M. Correlo, R. L. Reis, S. C. Kundu, *ACS Appl. Mater. Interfaces* **2019** , *11* , 14548.

[89] P. H. Tan, K. Z. Aung, S. L. Toh, J. C. Goh, S. S. Nathan,*Biomaterials* **2011** , *32* , 6131.

[90] P. H. Tan, S. S. Chia, S. L. Toh, J. C. Goh, S. S. Nathan,*J. Tissue Eng. Regener. Med.* **2016** , *10* , 637.

[91] K. Y. Lee, D. J. Mooney, *Prog. Polym. Sci* .**2012** , *37* , 106.

[92] R. Mhanna, J. Becher, M. Schnabelrauch, R. L. Reis, I. Pashkuleva, *Adv. Biosyst.* **2017** , *1* , e1700043.

[93] H. Malektaj, A. D. Drozdov, J. deClaville Christiansen, *Polymers* **2023** , *15,* 3012.

[94] K. Akeda, A. Nishimura, H. Satonaka, K. Shintani, K. Kusuzaki, A. Matsumine, Y. Kasai, K. Masuda, A. Uchida, *Oncol. Rep.***2009** , *22* , 997.

[95] I. Palubeckaitė, L. Crooks, D. P. Smith, L. M. Cole, H. Bram, C. L. Maitre, M. R. Clench, N. A. Cross, *J. Mass Spectrom.***2020** , *55* , e4461.

[96] C. J. Ke, K. H. Chiu, C. Y Chen, C. H. Huang, C. H. Yao,*Materials and Design* **2021** , *210* , 110109.

[97] M. Neufurth, X. Wang, H. C. Schröder, Q. Feng, B. Diehl-Seifert, T. Ziebart, R. Steffen, S. Wang, W. E. Müller,*Biomaterials* **2014** , *35* , 8810.

[98] P. M. Dana, J. Hallajzadeh, Z. Asemi, M. A. Mansournia, B. Yousefi, Int. J. *Biol. Macromo.* **2021** , *169* , 321.

[99] H.-Y. Yeh, J.-C. Lin, *J. Biomater. Sci. Polym. Ed* .**2008** , *19* , 291.

[100] D. W. Green, E.-J. Kim, H.-S. Jung, *J. Biomed. Mater. Res., Part A* **2015** , *103* , 2855.

[101] S. Dey, L. Laredj, K. Damjanovic, M. Muller, P. Beard, J. Gen. Virol. **2014** , *95* , 1539.

[102] S. K. L. Levengood M. Zhang, *J. Mater. Chem. B* ,**2014** , *2* , 3161.

[103] M. Assunção, D. Dehghan-Baniani, C. H. K. Yiu, T. Spater, S. Beyer, A. Blocki, *Front. Bioeng, Biotechnol.* , **2020** ,*8,* 602009.

[104] L. P. Ferreira, V. M. Gaspar, J. F. Mano, *Trends Biotechnol.* **2020** , *38* , 1397.

[105] A. Neishabouri, A. S. Khaboushan, F. Daghigh, A.-M. Kajbafzadeh, M. Majidi Zolbin, M. *Front. Bioeng. Biotechnol.***2022** , *10* , 805299.

[106] T. Hoshiba, *Materials* **2019** , *12* , 1311.

[107] J. Xu, S. Yang, Y. Su, X. Hu, Y. Xi, Y. Y. Cheng, Y. Kang, Y. Nie, B. Pan, K. Song, *Int. J. Bioprint.* **2022** , *9* , 10.

[108] A. Gilpin, Y. Yang, *Biomed Res. Int* . **2017** ,*2017* , 9831534.

[109] E. V. Isaeva, E. E. Beketov, N. V. Arguchinskaya, S. Ivanov, P. V. Shegay, D. Kaprin, *Sovrem. Tekhnologii Med* . **2022** ,*14* , 57.

[110] C.-F. Zhao Y. Wang, *J. Biomater. Tissue Eng.***2015** , *5* , 310.

[111] Y. Zhang, Y. Yao, Y. Zhang, *J. Visualized Exp.***2019** , *4,* e59271.

[112] E. M. Moore J. L. West, Regener. *Eng. Transl. Med.***2019** , *5* , 167.

[113] J. R. Choi, K. W. Yong, J. Y. Choi, A. C. Cowie,*Biotechniques* **2019** , *66* , 40.

[114] N. Rekowska, D. Arbeiter, H. Seitz, R. Mau, A. Riess, T. Eickner, N. Grabow, M. Teske, *Curr. Dir. Biomed. Eng* . **2022** , *8* , 181.

[115] E. Jabbari, S. K. Sarvestani, L. Daneshian, S. Moeinzadeh,*PLoS ONE* **2015** , *10,* e0132377.

[116] W. Zhu, N. J. Castro, H. Cui, X. Zhou, B. Boualam, R. McGrane, R. I. Glazer, L. G. Zhang, *Nanotechnology* **2016** ,*27* , 315103.

[117] E. Archer, M. Torretti, S. Madbouly, *Phys. Sci. Rev* .**2021** , *8* , 255.

[118] R. Dwivedi, S. Kumar, R. Pandey, A. Mahajan, D. Nandana, D. S. Katti, D. Mehrotra, *J. Oral Biol. Craniofac. Res* . **2020** ,*10* , 381.

[119] K. G. Nathan, K. Genasan, T. Kamarul, *Mar. Drugs* **2023** , *21* , 304.

[120] M. A. Teixeira, M. T. P. Amorim, H. P. Felgueiras, H. P.*Polymers* **2019** , *12* , 7. [121] A. Kumar, S. S. Han, *Int. J. Polym. Mater.***2017** , *66* , 159.

[122] W. Song, D. C. Markel, S. Wang, T. Shi, G. Mao, W. Ren,*Nanotechnology* **2012** , *23* , 115101.

[123] B. Pinto, A. C. Henriques, P. M. A. Silva, H. Bousbaa,*Pharmaceutics* **2020** , *12* , 1186.

[124] W. Mueller-Klieser, *J. Cancer Res. Clin. Oncol.***1987** , *113* , 101. [125] R. M. Sutherland, J. A. Mccredie, W. Rodger, *J. Natl. Cancer Inst.* **1971** , *46,* 113. [126] R. M. Sutherland, *Science* **1988** , *240* , 177. [127] A. S. Nunes, A. S. Barros, E. C. Costa, A. F. Moreira, I. J. Correia, *Biotechnol. Bioeng* . **2019** , *116* , 206. [128] B. N. S. OW, K. M, H. J, A. SSA, *Onco. Targets. Ther.***2016** , *9* , 7207. [129] S. Gunti, A. T. K. Hoke, K. P. Vu, N. R. London Jr,*Cancers* **2021** , *13* , 874.

[130] E. C. Costa, D. de Melo-Diogo, A. F. Moreira, M. P. Carvalho, I. J. Correia, *Biotechnol. J.* **2018** , *13* , 1700417.

[131] N. E. Timmins, L. K. Nielsen, *Methods in Molecular Medicine* , Humana Press, **2007** ; 141.[132] W. Kim, Y. Gwon, S. Park, H. Kim, J. Kim, *Bioact. Mater* . **2023** , *19* , 50. [133] E. C. Costa, D. de Melo-Diogo, A. F. Moreira, M. P. Carvalho, I. J. Correia, *Biotechnol. J* . **2018** , *13* , 1700417.

[134] G. W. West, R. Weichselbaum, J. B. Little, *Cancer Res.***1980** , *40* , 3665. [135] K. Arai, R. Sakamoto, D. Kubota, T. Kondo, *Proteomics***2013** , *13* , 2351. [136] M. Rimann, S. Laternser, A. Gvozdenovic, R. Muff, B. Fuchs, J. M. Kelm, U. Graf-Hausner, *J. Biotechnol.* **2014** ,*189* , 129.

[137] S. S. A. An, O. W. Seo, J. Lee, J. Hulme, N. Baek, *Drug Des., Dev. Ther.* **2016** , *10* , 2155. [138] I. E. Leon, A. L. D. Virgilio, V. Porro, C. I. Muglia, L. G. Naso, P. A. M. Williams, M. Bollati-Fogolin, S. B. Etcheverry,*Dalton Trans* . **2013** , *42* , 11868. [139] A. Kiss, A. P. Raduly, Z. Regdon, Z. Polgar, S. Tarapcsak, I. Sturniolo, T. El-Hamoly, L. Virag, C. Hegedűs, *Cancers***2020** , *12* , 1180.

[140] H. Chaddad, S. Kuchler-Bopp, G. Fuhrmann, H. Gegout, G. Ubeaud-Sequier, P. Schwinté, F. Bornert, N. Benkirane-Jessel, Y. Idoux-Gillet, *Exp. Cell Res.* **2017** , *360* , 138. [141] X. Guo, L. Yu, Z. Zhang, G. Dai, T. Gao, W. Guo, *Cancer Cell Int.* **2017** , *17* , 29.

[142] S. Ozturk, C. Gorgun, S. Gokalp, S. Vatansever, A. Sendemir,*Biotechnol. Bioeng.* **2020** , *117* , 2527. [143] C. P. Gibbs, V. G. Kukekov, J. D. Reith, O. Tchigrinova, O. N. Suslov, E. W. Scott, S. C. Ghivizzani,

T. N. Ignatova, D. A. Steindler,*Neoplasia* **2005** , *7* , 967. [144] M. Cortini, F. Macchi, F. Reggiani, E. Vitale, M. V. Lipreri, F. Perut, A. Ciarrocchi, N. Baldini, S. Avnet, *Cancers***2023** , *15* , 1221. [145] F. E. Freeman, R. Burdis, O. R. Mahon, D. J. Kelly, N. Artzi,*Adv. Healthcare Mater.* **2022** , *11,* 2101296. [146] S. Lenna, C. Bellotti, S. Duchi, E. Martella, M. Columbaro, B. Dozza, M. Ballestri, A. Guerrini, G. Sotgiu, T. Frisoni, L. Cevolani, G. Varchi, M. Ferrari, D. M. Donati, E. Lucarelli, *J. Exp. Clin. Cancer Res.* **2020** , *39* , 40.

[147] M. W. Tibbitt, K. S. Anseth, *Biotechnol. Bioeng* .**2009** , *103* , 655. [148] F. K. Lewns, O. Tsigkou, L. R. Cox, R. D. Wildman, L. M. Grover, G. Poologasundarampillai, *Adv. Mater* . **2023** ,*35* , e2301670.

[149] L. Z. Zhang, J. Mei, Z. K. Qian, X. S. Cai, Y. Jiang, W. D. Huang, *Pathol. Oncol. Res.* **2010** , *16* , 111.

[150] R. Elenjord, J. B. Allen, H. T. Johansen, H. Kildalsen, G. Svineng, G. M. Mælandsmo, T. Loennechen, J. O. Winberg, *FEBS J.***2009** , *276* , 5275. [151] T. Jiang, G. Xu, X. Chen, X. Huang, J. Zhao, L. Zheng,*Adv. Healthcare Mater.* **2019** , *8,* 2003129. [152] S. W. Sawyer M. E. Oest, *J. Tissue Sci. Eng.***2016** , *7* , 2. [153] F. Yang, J. Lu, Q. Ke, X. Peng, Y. Guo, X. Xie, *Sci. Rep.* **2018** , *8,* 7345.

[154] D. Gümbel, S. Bekeschus, N. Gelbrich, M. Napp, A. Ekkernkamp, A. Kramer, M. Stope, *Int. J. Mol. Sci.* **2017** , *18* , 2004.

[155] S. H. Shin, Y.J. Choi, H. Lee, H.-S. Kim, S.W. Seo,*Tumour Biol* . **2016** , *37* , 1591.

[156] A. Emami, T. Talaei-Khozani, S. Tavanafar, N. Zareifard, N. Azarpira, Z. Vojdani, *J. Transl. Med* . **2020** , *18* , 361. [157] A. Emami, T. Talaei-Khozani, Z. Vojdani, N. Zarei Fard,*J. Biomed. Mater. Res. B Appl. Biomater.* **2021** ,*109* , 19.

[158] T. Ono, R. Noguchi, Y. Yoshimatsu, Y. Sin, N. Kojima, T. Kondo, *J. Electrophor* . **2021** , *65* , 33. [159] M. V. Monteiro, V. M. Gaspar, L. P. Ferreira, J. F. Mano,*Biomater. Sci.* **2020** , *8* , 1855. [160] C. F. Monteiro, C. A. Custódio, J. F. Mano, *Acta Biomater.* **2021** , *134* , 204. [161] J. Xue, T. Wu, Y. Dai, Y. Xia, *Chem. Rev.***2019** , *119* , 5298.

[162] A. Haider, S. Haider, I.-K. Kang, *Arab. J. Chem.***2018** , *11* , 1165. [163] S.-W. Tsai, H.-M. Liou, C.-J. Lin, K.-L. Kuo, Y.-S. Hung, R.-C. Weng, F.-Y. Hsu, *PLoS ONE* **2012** , *7* , e31200.

[164] F. Fahimipour, E. Dashtimoghadam, M. Mahdi Hasani-Sadrabadi, J. Vargas, D. Vashaee, D. C. Lobner, T. S. Jafarzadeh Kashi, B. Ghasemzadeh, L. Tayebi, *Dent. Mater.* **2019** , *35* , 990. [165] L. M. Lawrence, R. R. Salary, V. Miller, A. Valluri, K. L. Denning, S. Case-Perry, K. Abdelgaber, S. Smith, P. P. Claudio, J. B. Day, *Int. J. Mol. Sci* . **2023** , *24,* 4940.

[166] A. Pössl, D. Hartzke, P. Schlupp, F. E. Runkel, *Appl. Sci* . **2021** , *12* , 326. [167] S. Dani, T. Ahlfeld, F. Albrecht, S. Duin, P. Kluger, A. Lode, M. Gelinsky, *Gels* **2021** , *7* , 227. [168] R. Staros, A. Michalak, K. Rusinek, K. Mucha, Z. Pojda, R. Zagożdżon, *Cancers* **2022** , *14,* 3126.

[169] N. Khoshnood, A. A. *Bioprinting* **2020** ,*19* , e00088.

[170] M.-L. Wang, N.-Y. Xu, R.-Z. Tang, X.-Q. Liu, *Mater. Today Bio* **2022** , *15* , 100295.

[171] S. Derakhshanfar, R. Mbeleck, K. Xu, X. Zhang, W. Zhong, M. Xing, *Bioact. Mater* . **2018** , *3* , 144. [172] S. Mao, Y. Pang, T. Liu, Y. Shao, J. He, H. Yang, Y. Mao, W. Sun, *Biofabrication***2020** , *12* , 042001. [173] R. Augustine, S. N. Kalva, R. Ahmad, A. A. Zahid, S. Hasan, A. Nayeem, L. McClements, A. Hasan, *Transl. Oncol* . **2021** ,*14* , 101015.

[174] B. Grigoryan, D. W. Sazer, A. Avila, J. L. Albritton, A. Padhye, A. H. Ta, P. T. Greenfield, D. L. Gibbons, J. S. Miller,*Sci. Rep* . **2021** , *11* , 317.

[175] X. Wang, E. Tolba, H. C. Der, M. Neufurth, Q. Feng, B. R. Diehl-Seifert, W. E. M. Ller, *PLoS ONE* , **2014** , *9,*e112497. [176] Y. B. Kim, H. Lee, G. H. Kim, *ACS Appl. Mater. Interfaces* **2016** , *8* , 32230. [177] N. Diamantides, L. Wang, T. Pruiksma, J. Siemiatkoski, C. Dugopolski, S. Shortkroff, S. Kennedy, L. J. Bonassar,*Biofabrication* **2017** , *9* , 034102. [178] E. O. Osidak, V. I. Kozhukhov, M. S. Osidak, S. P.

Domogatsky,*Int. J. Bioprinting* **2020** , *6* , 270. [179] E. Pellegrini, G. Desando, M. Petretta, A. Cellamare, C. Cristalli, M. Pasello, M. C. Manara, B. Grigolo, K. Scotlandi,*Polymers* **2022** , *14* , 4070. [180] Y. Lin, Y. Yang, K. Yuan, S. Yang, S. Zhang, H. Li, T. Tang,*Bioact. Mater.* **2022** , *18* , 459.

[181] G. Loi, G. Stucchi, F. Scocozza, L. Cansolino, F. Cadamuro, E. Delgrosso, F. Riva, C. Ferrari, L. Russo, M. Conti, *Gels***2023** , *9* , 129. [182] S. Swaminathan, Q. Hamid, W. Sun, A. M. Clyne,*Biofabrication* **2019** , *11* , 025003. [183] N. C. Negrini, C. Ricci, F. Bongiorni, L. Trombi, D. D'Alessandro, S. Danti, S. Farè, *Cancers* **2022** ,*14* , 2003.

[184] L. Y. Yeo, H.-C. Chang, P.P.Y. Chan, J.R. Friend, *Small***2011** , *7* , 12.

[185] M. Huang, S. Fan, W. Xing, C. Liu, *Math. Comput. Model* .**2010** , *52* , 2036

[186] M.R. Carvalho, D. Lima, R.L. Reis, V.M. Correlo, J.M. Oliveira, *Trends Biotechnol* . **2015** , *33* , 667.

[187] S. Sarkar, C.-C. Peng, Y.-C. Tung, *PLoS One***2020** , *15* , e0240833.

[188] D. Wei, J. Sun, J. Bolderson, M. Zhong, M.J. Dalby, M. Cusack, H. Yin, H. Fan, X. Zhang, A*CS Appl. Mater. Interfaces***2017** , *9* , 14606.

[189] OrganoPlate® Graft. https://www.mimetas.com/en/organoplate-graft/, accessed: August,**2023** . [190] G. Colella, F. Fazioli, M. Gallo, A. De Chiara, G. Apice, C. Ruosi, A. Cimmino, F. de Nigris, *Int. J. Mol. Sci.* **2018** ,*19* , 615.

[191] J. Ma, Y. Wang, J. Liu, *RSC Adv.* **2018** ,*8* , 21712.

[192] A. Aung, J. Theprungsirikul, H.L. Lim, S. Varghese, *Lab on a Chip* 2016, *16* , 1886. [193] S. Xu, S. Tan, K. Guo, *Cancers (Basel)* **2023** ,*15* , 17. [194] I. Psilopatis, S. Kokkali, K. Palamaris, A. Digklia, K. Vrettou, S. Theocharis, *Int. J. Mol. Sci* . **2022** ,*23* , 11271.

[195] S. Yang, H. Hu, H. Kung, R. Zou, Y. Dai, Y. Hu, T. Wang, T. Lv, J. Yu, F. Li, *MedComm* **2023** , *4* , e274. [196] A. Y. Parikh, R. Masi, B. Gasmi, K.-I. Hanada, M. Parkhurst, J. Gartner, S. Sindiri, Prickett, P. Robbins, N. Zacharakis, M. Beshiri, K. Kelly, S. A. Rosenberg, J. C. Yang, *Cancer Immunol. Immunother.* **2023** , *72* , 3149. [197] W. S. Chan, X. Mo, P. P. C. Ip, K. Y. Tse, *Cancer Med* .**2023** , *12* , 19714. [198] J. M. Rosenbluth, R. C. J. Schackmann, G. K. Gray, L. M. Selfors, C. M.-C. Li, M. Boedicker, H. J. Kuiken, A. Richardson, J. Brock, J. Garber, D. Dillon, N. Sachs, H. Clevers, J. S. Brugge, J. S.*Nat. Commun* . **2020** , *11* , 1711.

[199] A. He, Y. Huang, W. Cheng, D. Zhang, W. He, Y. Bai, C. Gu, Z. Ma, Z. He, G. Si, B. Chen, D.T. Breault, M. Dong, D. Xiang, *Med. Oncol.* **2020** , *37* , 105. [200] S. Johansson, *Dissertation* , Uppsala University**2019** .

[201] J. A. Somarelli, G. Rupprecht, E. Altunel, E. M. Flamant, S. Rao, D. Sivaraj, A. L. Lazarides, S. M. Hoskinson, M. U. Sheth, S. Cheng, S. Y. Kim, K. E. Ware, A. Agarwal, M. M. Cullen, L. E. Selmic, J. I. Everitt, S. J. McCall, C. Eward, W. C. Eward, D. S. Hsu,*Cancers* **2020** , *12* , 3335.